Can a single valence electron alter the electrocatalytic activity and selectivity for CO$_2$ reduction on the subnanometer scale?

Raju, Rajesh Kumar; Rodriguez, Paramaconi; Johnston, Roy L.

[Link to publication on Research at Birmingham portal](#)

Can a single valence electron alter the electrocatalytic activity and selectivity for CO_2 reduction at the subnanometre level?

Rajesh Kumar Raju[a*], Paramaconi Rodriguez[a] and Roy L. Johnston[a*]

[a] School of Chemistry, University of Birmingham, Edgbaston, Birmingham B15 2TT, United Kingdom

* r.l.johnston@bham.ac.uk, rajesh444@gmail.com

Abstract

Electrocatalytic reduction of CO_2 (CO2RR) is an excellent strategy for addressing both the issue of ever-increasing anthropogenic CO_2 emissions as well as the rapid diminishing of non-renewable fossil reserves. Recently, significant attention has focussed on the development of size-selected subnanometre nanocatalysts because of the unique electronic, geometric and catalytic properties of these clusters, which often exhibit enhanced catalytic activities and selectivities compared to bulk metal catalysts and larger nanoparticles. In this paper, we investigate in detail the electrocatalytic activity of size-selected Cu_n clusters (n=3-6) employing the Computational Hydrogen Electrode (CHE) model. We have found a striking similarity between CO2RR activity of Cu_3 and Cu_5 and between Cu_4 and Cu_6 nanoclusters. The reaction proceeds through $* + CO2 \rightarrow COOH* \rightarrow CO* + H_2O \rightarrow CHO* \rightarrow CH_2O* \rightarrow CH_3O* \rightarrow O* + CH_4 \rightarrow OH* \rightarrow * + H_2O$ as in the case of copper surface on all the Cu clusters. The rate-limiting potential on Cu_4 and Cu_6 clusters is the proton-electron ($H^+ + e^-$) transfer to CO* to form the CHO* adsorbed species, which is also the rate-limiting step on Cu surfaces, whilst on Cu_3 and Cu_5 clusters it is the removal of the adsorbed OH* from the cluster surface (OH* $\rightarrow$ * + H_2O). Most importantly, we have identified a general trend in the exergonicity and endergonicity of each step with the spin-state of the nanocluster. In general, electrochemical steps corresponding to an odd total number of ($H^+ + e^-$) pair transfers, leading to the formation of the doublet adsorbed species on Cu_4 and Cu_6 clusters, are highly endergonic uphill processes relative to the same steps on Cu_3 and Cu_5 clusters. However, steps corresponding to an even total number of proton-electron pair transfers, leading to the formation of the singlet adsorbed species on Cu_4 and Cu_6 clusters, are highly exergonic downhill process relative to the same steps on Cu_3 and Cu_5. We have also found that the competing hydrogen evolution reaction (HER) is more hindered on Cu_3 and Cu_5 compared to Cu_4 and Cu_6 clusters. There is also a general qualitative relationship between the exer/endergonicity of an electrochemical step and the HOMO-LUMO gap of the various cluster-adsorbate complexes. We have found that an increase or decrease of a single valence electron can significantly alter the electrocatalytic activity and reactivity at the subnanometre level and this has great implications in the design and development of size-selected nanoclusters for CO2RR and similar reactions.

Introduction

Anthropogenic CO_2 emissions pose a serious threat to human-kind concerning global warming and climate change. Another serious concern is the rapid depletion of fossil fuel resources that may lead to a significant energy crisis in the future. In fact, large-scale combustion of fossil fuels is the major source of anthropogenic CO_2 emissions. The average CO_2 concentration in the atmosphere has already surpassed 400 ppm and is 120 ppm higher than the pre-industrial historical level of 290 ppm.[1] The adverse consequence of these ever-increasing emissions on climate change is also evident. According to data from the NOAA National Centres for Environmental Information, all years in the 21st century (2001-2017) rank amongst the hottest years on record; and 2015, 2016, and 2017 stand in the top three positions.[2] CO_2 emissions and global warming are expected to increase further because of growing energy demand worldwide due to population and industrial growth. The development of low-cost, clean, efficient and sustainable alternative energy resources with minimal environmental impact is of paramount interest. In this context, recycling of CO_2 emitted from sources such as industry into useful chemicals, especially fuels, is an ideal solution which addresses both the issues of ever-increasing CO_2 emissions and diminishing non-renewal energy resources.

Despite the fact that CO_2 is an inexpensive, abundant and renewable C1 source for synthesising many useful chemicals, the activation and subsequent chemical transformation of CO_2 is a formidable challenge due to its chemical inertness, as the carbon atoms are in their highest oxidation state. Of the many possible reduction products, CO and methane (CH_4) find applications as gaseous fuels and formic acid (HCOOH) and methanol (CH_3OH) find applications as liquid fuels.[3,4] There have been a number of heterogeneous catalysts with different supports and promoters reported for the direct hydrogenation of CO_2 with H_2.[5–7] However, these heterogeneous catalysts exhibit some serious drawbacks, such as high operating temperatures and pressures (typically above 200°C and 50-100 atm. pressures), lack of catalyst tuning and formation of undesirable by-products. Electrochemical reduction of CO_2 (CO2RR) is an alternative way of achieving CO_2 reduction and has the distinct advantage that it operates at room temperature and atmospheric pressure. Moreover, the electrocatalytic activity and selectivity can be easily controlled by adjustment of the electrode potentials. There are numerous excellent reviews in the literature on different types of electrode materials (pure metals, alloys, oxides, organic, clusters etc.), their stability, activity and product selectivity etc.[8–16] In recent decades, most of the research effort has been devoted to the development of metal electrodes for the electrocatalytic reduction of CO_2. These metal catalysts are divided into different distinct groups: namely CO-selective metals (e.g.; Au, Ag, Zn and Pd), formate-selective metals (e.g., Pb, Hg, In, Sn, Bi and Cd) and hydrogen-selective metals (e.g. Fe, Ni, Pt and Ti), based on their tendency to bind various intermediates and reduction products.[8–16] Although many different materials have been proposed, electrodes primarily based on noble metals (e.g. Pd, Pt, Cu, Ag and Au) are commonly used in CO2RR reactions. However, none of these metals have proved successful in large-scale conversion, in terms of efficiency and selectivity.

Copper is the only metal that has been experimentally shown to catalyse reduction beyond the two-electron reduction stage and to produce higher reduction products such as alcohols and hydrocarbons, in particular CH_4, from CO2RR.[17–24] None of the metals studied so far have shown the ability to reduce CO_2 to methanol in significant yield.[11] As the CO2RR reaction is usually carried out in aqueous media, the CO2RR has to compete with the hydrogen evolution reaction (HER), which is also a cathodic side reaction and has much lower overpotential on most metallic surfaces.[25,26] Hori *et al.* reported from their experimental studies that hydrocarbons (CH_4 and C_2H_4) are the dominant reduction products at sufficiently large negative potentials, whereas at lower potentials, H_2, CO and HCOOH are dominant[18,22]. Nørskov and co-workers provided the first theoretical insight into copper's unique ability to reduce CO_2 into hydrocarbons, employing the Computational Hydrogen Electrode (CHE) model for the Cu(211) surface.[27] They found that the transfer of a proton-electron pair to the adsorbed CO species (CO*) to form adsorbed CHO (CHO*) is the key-limiting step in the production of the hydrocarbons and the lowest energy route to methane is $* + CO_2 \rightarrow COOH* \rightarrow CO* + H_2O \rightarrow CHO* \rightarrow CH_2O* \rightarrow CH_3O* \rightarrow O* + CH_4 \rightarrow OH* \rightarrow * + H_2O$ [where * indicates an adsorption site on the surface of the catalyst]. Consistent with experimental observations, their theoretical work also found that

hydrocarbon formation takes place only at a higher applied potential (-0.74 V). Based on theoretical studies, Asthragiri and co-workers proposed an alternative path: $* + CO_2 \rightarrow COOH* \rightarrow CO* + H_2O \rightarrow COH \rightarrow C* \rightarrow CH* \rightarrow CH_2* \rightarrow CH_3* \rightarrow * + CH_4$, in which the reaction proceeds via a hydroxymethylidyne (COH) intermediate.[28,29] A recent experimental study by Kuhl *et al.* identified a total of 16 different CO_2 reduction products, including a wide range of C_1-C_3 species (with five detected for the first time) and proposed a reaction scheme involving enol-like intermediates for the production of multicarbon products.[30] Recently, Garza *et al*. have proposed a mechanism for the electroreduction of CO_2 to C_2 products on Cu surface, based on DFT calculations.[31] A number of theoretical studies have been carried out to explain the formation of mono- and multicarbon products from CO_2 reduction, as reported by various research groups.[32–37]

Recently, catalysis by metal nanoparticles ("nanocatalysis") has gained significant attention owing to the high activity and selectivity as well as low metal cost of nanoparticles (NPs) compared to the traditional bulk metal catalysts.[38,39] The cluster size (subnanometre or NPs), shape and high surface-to-volume ratio (compared to bulk metals) of nanoclusters impart unique electronic effects, surface chemistry and catalytic properties to nanocatalysts.[40] The increased density of exposed low-coordinated unsaturated sites presents a larger number of catalytically active sites for the reactant species. Subnanometre clusters (size-selected nanoclusters of few atoms) show particular promise in the field of nanocatalysis, as the addition or removal of a single atom can induce substantial changes in the electronic, geometric and catalytic properties of the subnanometre cluster, which are entirely different from larger nanoclusters or bulk materials.[41–48] The particle size effect on CO2RR has been investigated for metal NPs of Au, Ag, Bi, Pd, , Ni, and Sn and it was found in general that NPs with different sizes exhibit different CO2RR activity and selevtivity.[49–57] Tang *et al.* reported that Cu NP-covered electrodes exhibit better selectivity towards hydrocarbon production from CO_2 electroreduction, compared with electropolished and argon-sputtered Cu electrodes.[58] Strasser *et al.* investigated the particle size effect of Cu NPs on CO2RR and found that as the particle size decreases, in particular below 5 nm, the activity and selectivity for H_2 and CO increases dramatically.[59] Vajda *et al.* have investigated the electrochemical behaviour of Cu_5 and Cu_{20} nanoclusters in the presence of N_2 and CO_2 and found different redox behaviour for Cu_5 and Cu_{20} nanoclusters.[60] Cu NPs supported on glassy carbon have been shown to achieve four times larger methanation current densities compared to high-purity Cu foil electrodes and exhibit a Faradaic efficiency of 80%. Similarly, the Au_{25} cluster exhibits a significant enhancement of the $CO_2 \rightarrow CO$ reaction over large Au NPs and the bulk Au surface.[51] Mistry *et al* reported that the current density for $CO_2 \rightarrow CO$ increases drastically with decreasing Au nanoparticle size.[49] Studies on Ag nanoparticle catalysts show that the $CO_2 \rightarrow CO$ conversion rate is approximately 10 times higher on 5 nm Ag nanoparticles than on bulk silver.[53] Similarly, Kim *et al.* have reported significant decrease of overpotential and a 4-fold increase in the CO Faradaic efficient with the optimal Ag NP size of 5nm compared to polycrystalline Ag foil.[52] Gao et. al. investigated the size-depended electrocatalytic selectivity for CO formation on Pd NPs with different sizes and reported that the Faradaic efficiency for CO production shows significant enhancement (5.8% over 10.3 nm NPs to 91.2% over 3.7 nm NPs), along with an 18.4-fold increase in current density.[54] Similarly, nanostructured Sn catalysts have been shown to produce formate at overpotentials as low as 340 mV.[57] Downsizing the NPs to a single atom, the ultimate size limit for subnanometre clusters, has opened a novel area in catalysis termed "single-atom catalysis" (SAC).[61,62] In a recent study, Zhao *et al.* showed that Ni SAC can reduce CO_2 to CO with excellent Faradaic efficiency and current density.[56] The use of single-atomic Cu on ceria (with multiple oxygen vacancies) was recently reported for electrocatalytic reduction of CO_2 to methane.[63] Jia M *et al.* have provided a review that highlights the recent progress in the development of single-atom catalysts for the electroreduction of CO_2.[64] Back S. *et al.* employing computational approach have provided deep theoretical insights into the single transition metal atoms anchored on defective graphene with single and double vacancies for CO_2 electroreduction.[65] Duff *et al.* have investigated the surface coverage of the oxygen species, a surface-structure and potential dependent factor on product selectivity of CO_2 electroreduction to alcohols and carbonyls on Cu electrodes.[66] Besides electrocatalytic CO_2 reduction, direct hydrogenation of CO_2 to methanol (thermal catalysis) on small size-selected Cu_n clusters (n=3, 4, 20) supported on Al_2O_3 thin films has been reported by Vajda and co-

workers.[67,68] They found that catalytic activity for methanol synthesis varies with cluster size in the order Cu_4 > Cu_{20} > Cu_3 and Cu_4 is the most active low-pressure catalyst for CO_2 hydrogenation to CH_3OH. The removal of one atom from Cu_4 to Cu_3 cluster reduces the activity of CH_3OH production drastically, by more than 50%. They also reported charge states (prior to reduction) of 1.8, 1.7 and 1.6 at 25 °C for Cu_3, Cu_4 and Cu_{20} clusters, respectively, and identified that the reduction temperature decreases with increasing cluster size.

Despite recent advances in computational methodologies, there have been relatively few theoretical studies reported for electrocatalytic reduction of CO_2 on nanoclusters. Several DFT studies have been reported for the electroreduction of CO_2 on larger clusters, such as Au_{38} and Au_{55},[49] Pd_{38} and Pd_{55},[54] ligand-protected $Au_{25}(SCH_3)_{18}{}^q$ (charge q = -1, 0, +1) clusters,[50,51] Cu_{85},[69] and Cu_{79}.[70] Computational studies on the CO2RR activity of subnanometre transition metal clusters are also limited. Liu *et al.* investigated the electroreduction of CO_2 to CO, HCOOH, and CH_4 on a number of tetra-atomic metal clusters and found that the overpotentials for forming CH_4 are in the order Co_4 < Fe_4 < Ni_4 < Cu_4 < Pt_4.[71] In a very recent computational study of subnanometre Cu clusters, Shanmugam *et al.* reported that Cu atoms at two-coordination sites are more selective for reduction of CO_2 to CO at a lower applied voltage compared to higher coordination sites.[72] Apart from this limited number of studies, no systematic evaluation has been made of the effect of cluster size and electronic state of the Cu clusters on their CO2RR activity and selectivity towards the higher reduction products such as CH_4 vs CH_3OH.

In this study, we investigate in detail the catalytic ability of subnanometre Cu_n (n = 3-6) clusters to reduce CO_2 electrochemically and their relative activity and selectivity towards various reduction products, in particular for higher reduction products. We have chosen these four clusters as they represent two pairs of subnanometre clusters with quite different electronic states: odd numbers of electrons (Cu_3 and Cu_5); and even numbers of electrons (Cu_4 and Cu_6). As the size of the clusters are significantly smaller, we expect that quantum size effects will come into play and even a difference of a single electron can impart significant changes in the electrocatalytic activity. We use the computational hydrogen electron model (CHE) of Nørskov[27,73], at the DFT level, to investigate the electrocatalytic pathways for these Cu clusters via CHO* and COH* adsorbed species: the two lowest-energy routes proposed for the CO2RR on the Cu surface, as well as evaluating the theoretical overpotential for the CO2RR on these clusters. This study will shed light into the electronic and geometrical factors that govern the course of the CO2RR on subnanometre clusters, as well as providing a theoretical platform for the further development of novel robust subnanometre cluster-based catalysts for the electroreduction of CO_2 to fuels.

Computational Details:

(i) Structural optimisation of Cu_n (n=3-6) clusters

An extensive search for global minimum energy geometries was performed for Cu_n (n=3-6), employing the Birmingham Parallel Genetic Algorithm (BPGA) at the DFT level.[74,75] BPGA employs a pool methodology to evaluate the geometries in parallel. In each run, multiple BPGA instances are implemented and, in each instance, the GA operations and local energy minimisations are performed across multiple cores. Initially, a number of random geometries are generated (10 in this study) and DFT minimisations are performed on these geometries to form the initial pool population. Subsequently, GA crossover and mutation operations are performed on pairs (crossover) or individual (mutation) members of the population. The crossover operation involves selecting a pair of clusters from the pool using the tournament selection method, based on the fitness criterion: the fittest isomers (clusters with the lowest energies) are more likely to be selected for crossover. Offspring structures are then generated using the cut-and-splice method of Deaven and Ho.[76] A single cluster chosen at random for the mutation operation, achieved by displacing some of the atoms randomly or introducing a new, randomly generated cluster). After crossover and mutation operations, these new structures are then locally minimised at the DFT level and their energies are compared with the existing structures in the pool. New, low-energy structures replace higher energy pool members. The BPGA program is run until convergence is achieved. In each run, 400 structures are minimized and if the energy of the lowest

energy structures in two successive runs are within 10^{-4} eV, we assume that convergence is attained. In this study, these lowest energy structures in the two successive runs are essentially the same.

All the local energy minimisations in the GA were performed using Gamma-point spin-polarized DFT calculations employing a plane wave basis set within the Vienna ab initio Simulation Package (VASP).[77–80] Spin-states were optimized within VASP independently for each structure from BPGA during global optimization, using projected-augmented wave (PAW)[81] pseudopotentials and the Perdew-Burke-Ernzerhof (PBE)[82] GGA exchange-correlation functional. A plane-wave cut-off energy of 400 eV was used and Methfessel-Paxton[83] smearing with a sigma value of 0.01 eV to improve convergence.

(ii) CO_2RR electro catalytic reduction studies

The global minima determined from the BPGA for Cu_n (n=3-6) nanoclusters, as well as various adsorbed species on the Cu clusters (CO_2*, $COOH*$, $CO*$, $CHO*$, CH_2O*, CH_3O*, $C(OH)_2*$, $COH*$, $CHOH*$, CH_2OH*, $C*$, $CH*$, CH_2*, CH_3*, $OOCH*$, $O*$, $OH*$, $H*$), and free molecules (CO_2, H_2, H_2O, CO, $HCOOH$, CH_3OH and CH_4) were geometry optimised using orbital-based DFT within the Gaussian09 program.[84] These geometry optimization calculations were performed using the long-range corrected hybrid density functional with empirical atom-atom dispersion correction ωB97XD[85] and the def2SVPP basis set.[86,87] These were followed by a single-point energy calculation using the larger def2-TZVPP basis set.[86,87] Stability analysis of the wavefunctions of the optimized geometries have been carried out to make sure that the wavefunctions are stable and there are no spin crossovers and no tendency for open-shell singlets. For each of the free clusters and cluster-adsorbates, in addition to the lowest electronic state (singlet or doublet depending on the number of unpaired electrons), we searched the minima on two higher-spin electronic surfaces (triplet and quintet or quartet and sextet). We have validated the performance of the ωB97XD functional with respect to high-level CCSD(T) calculations for the CO_2RR studies and we have also investigated the basis set dependence of the cluster geometries and energies (See supplementary information for more details).

Free energy changes (ΔG) for various electrochemical steps were then calculated using the Computational Hydrogen Electrode Model (CHE) developed by Nørskov and co-workers.[27,73] Thermal corrections (using harmonic vibrational frequencies) were computed at the ωB97XD/def2SVPP level and solvent (water) effects were included using the implicit universal solvation model (SMD) for the lowest-energy geometries of each of the adsorbed species.[88] Free energy values without solvent correction were also computed for a direct comparison with gas phase results. For CO_2 adsorption studies, we have found that the free energy of adsorption is not always larger (most negative) for the lowest energy gas-phase geometries. Considering this fact, we have included the preferred lowest energy geometry for CO_2 adsorbed species separately in the gas-phase and in water. For some of the cluster-adsorbed species, we have found geometry changes in water compared to the gas phase. Charges on cluster atoms were calculated using the Natural Bond Orbital (NBO) analysis.[89]

According to the CHE model, the free energy change for an electrochemical step can be calculated as:

$$\Delta G[A* + (H^+ + e^-) \rightarrow AH*] = \mu(AH*) - \mu(A*) - [\mu(H^+) + \mu(e^-)] \qquad [1]$$

In the CHE model, the chemical potential of the (H+/e-) pair is equal to half the chemical potential of the gas-phase H_2 molecule. The total chemical potential of the proton-electron pair as a function of applied potential U, at all temperatures, can be calculated as:

$$\mu(H^+) + \mu(e^-) = 0.5 \, \mu(H_2(g)) - eU \qquad [2]$$

At zero applied potential (U = 0 V), ΔG becomes $-U_L/e$, where U_L is the limiting potential. The CHE model ignores the kinetic barriers for (H+/e−) pair transfers to adsorbate species as the barriers for proton transfer to adsorbed species are assumed to be small enough to be surmountable at room temperatures. This assumption is supported by previous studies on the proton transfer barriers for the reduction reactions of O_2 to OOH and OH to H_2O on Pt which show that these barriers lie in the range 0.15-0.25 eV for zero applied

potential and decrease with increasing applied voltage.[90,91] CHE model studies of CO2RR assume that the extent to which the CO2RR reaction is favoured on different surfaces can be simply predicted by calculating the thermodynamic changes of the individual electrochemical steps. In other words, the reaction free energy changes for various electrochemical steps can be used as a catalytic descriptor for the favourability of the CO2RR on various surfaces. Further details about the computational details can be found in the Supplementary Information.

Results and Discussions

Structure Characterization of Cu$_n$ (n=3-6) clusters

As the size and shape of the nanoclusters are critical in the CO$_2$RR activity, the first step was to identify the most stable geometrical arrangement of these clusters. We have made an extensive search for the most stable geometrical configuration for these nanoclusters employing BPGA. The Cu$_3$ cluster adopts an isosceles triangle geometry with C$_{2v}$ symmetry, Cu$_4$ has a rhombus configuration with D$_{2h}$ symmetry. The other two Cu clusters Cu$_5$ and Cu$_6$ also adopts planar configurations, with C$_{2v}$ and D$_{3h}$ symmetries, respectively. All of these structures are fragments of a 2D close packed network and the 3-5 atom clusters can be formed from the triangular Cu$_6$ structure by the removal of one or more atoms. The geometry of the nanoclusters, with the symmetry-equivalent atoms indicated, are shown in Figure 1, along with the unique Cu-Cu bond lengths and NBO atomic charges. These Cu cluster structures are all in agreement with previously reported geometries for these sizes.[92]

Following the BPGA optimisation and subsequent reoptimisation at ωB97XD level, all the bare Cu clusters (Cu$_3$–Cu$_6$) were found to adopt the lowest possible spin-state, with Cu clusters containing an even number of electrons (Cu$_4$ and Cu$_6$) in the singlet-state and those with an odd number of electrons (Cu$_3$ and Cu$_5$) in the doublet state. Although, we are not expecting a cross-over to higher spins on binding organic adsorbates, we have performed extensive searches for the minimum energy structures for the adsorbates on higher spin-states. For cluster-adsorbates with odd numbers of electrons such as CO$_2$* on Cu$_3$ and Cu$_5$ clusters and CH* on Cu$_4$ and Cu$_6$, we performed geometry searches on doublet, quartet and sextet electronic states. Similarly, for cluster-adsorbates with even numbers of electrons such as CH* on Cu$_3$ and Cu$_5$ clusters and CO$_2$* on Cu$_4$ and Cu$_6$, geometric searchers were performed on singlet, triplet and quintet electronic states. Many different initial starting positions for the adsorbed molecules and molecular fragments were chosen for geometry optimisation, corresponding to the various symmetry-inequivalent atomic and edge sites of the cluster, in order to locate the most stable adsorbate geometries. For example, for Cu$_5$ we optimised the different adsorbed species on atoms Cu(a), Cu(b) and Cu(c) and on the edges Cu(a)-Cu(b), Cu(b)-Cu(c), Cu(a)-Cu(c) and Cu(c)-Cu(c) (See Figure 1). Similarly, for Cu$_4$ and Cu$_6$, which have higher symmetry, we optimised the adsorbates on Cu atoms a and b and edges Cu(a)-Cu(b) and Cu(b)-Cu(b) (See Figure 1). In all cases, the optimization converged to a number of distinct minimum energy structures for the same adsorbed species and we have chosen only the lowest-energy structure for further CO$_2$RR studies. As we expected, we have found that cluster-adsorbate complexes in the higher spin states are thermodynamically highly unstable compared to the lowest spin-states (singlets or doublets). We have chosen the adsorbed species involved in the lowest energy reaction pathways via the CHO* and COH* species proposed by Nørskov *et al.* and Asthagiri *et al.* on the metallic copper surface.[27–29] Moreover, the computational studies by Liu *et al.* showed that the lowest energy CO2RR pathways on the tetra-atomic clusters Fe$_4$, Co$_4$, Ni$_4$, Cu$_4$ and Pt$_4$ also proceed via the CHO* pathway,[62] in agreement with Nørskov's results for the Cu(211) surface.[28]
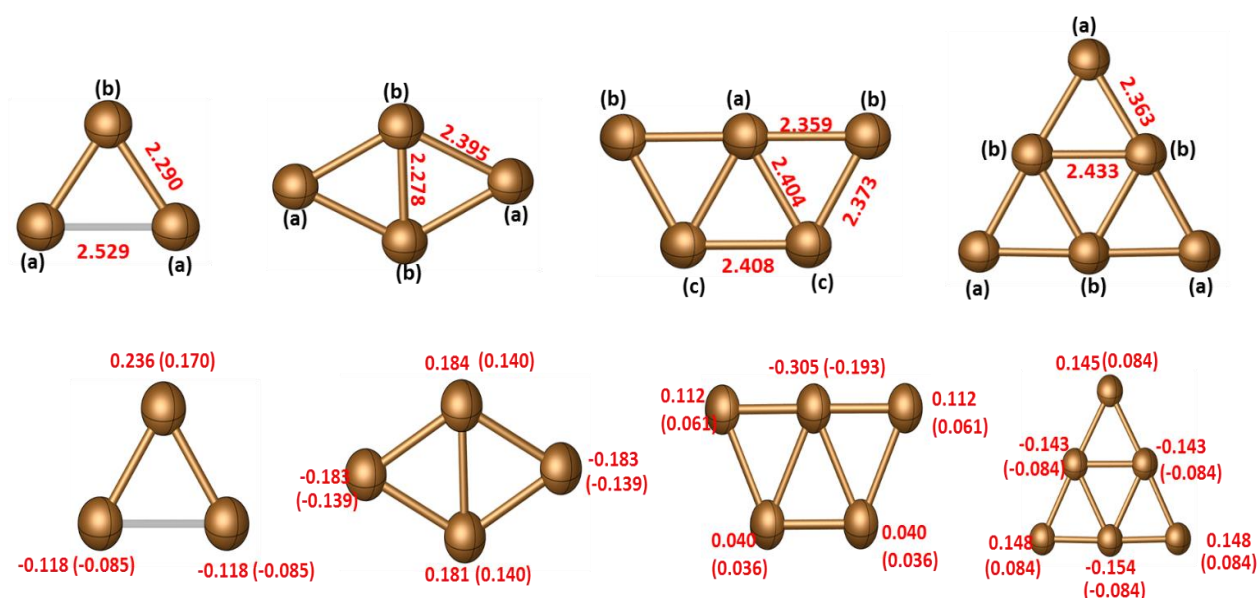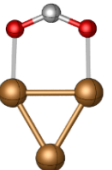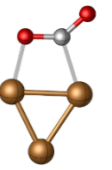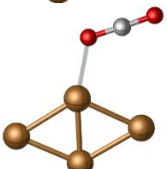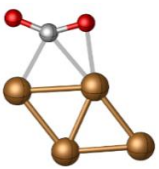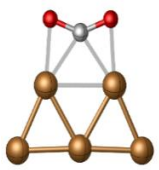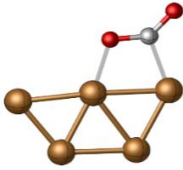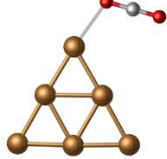
Figure 1: Lowest energy geometrical configurations for the Cu_3 (C_{2v}), Cu_4 (D_{2h}), Cu_5 (C_{2v}) and Cu_6 (D_{3h}) clusters optimized at the ωB97XD/def2-SVPP level. In the top row, the different symmetry-equivalent atomic positions are labelled (a), (b), and (c) and unique Cu-Cu bond lengths (Å) are marked. In the bottom row, the NBO atomic charges are given for the solvated clusters and (in parentheses) for the clusters in the gas phase.

Table 1: Adsorption free energies (ΔG_{ads} / eV) and geometries of the CO_2* (CO_2-adsorbed complexes) for different Cu_n (n=3-6) clusters in the gas-phase and water. The net NBO charge on the adsorbed CO_2 molecule (q_{CO2}) are also listed.

Cluster	Gas-Phase			Water		
	Geometry	ΔG_{ads}	q_{CO2}	Geometry	ΔG_{ads}	q_{CO2}
Cu_3		0.072	-0.703		-0.940	-0.882
Cu_4		0.072	+0.071		-0.483	-0.844
Cu_5		0.093	-0.520		-0.680	-0.875
Cu_6		0.175	+0.033		-0.077	+0.010

CO$_2$ adsorption on Cu clusters:

CO$_2$ can form a number of distinct cluster-bound complexes by interacting in different binding modes on the various symmetry-inequivalent atoms (atop or terminal binding sites) and Cu-Cu edges (bridging sites) on the clusters. An extensive search has been made to locate the lowest energy minima for the CO$_2$-Cu clusters complexes and the lowest energy geometry was selected for further investigation. The free energies of adsorption (ΔG_{ads}) for the lowest energy geometries of the CO$_2$-cluster complexes are given in Table 1, both in the gas phase and in (implicit) water.

(i) Gas-phase clusters: The adsorption free energies of CO$_2$ on all the Cu clusters are positive in the gas-phase, which means that gas-phase adsorption of CO$_2$ is thermodynamically unfavourable. For Cu$_4$, CO$_2$ is physisorbed via one of the oxygen atoms to Cu(b), which has a positive NBO charge of +0.140. For Cu$_6$, again CO$_2$ is physisorbed via a single O-Cu interaction (analogous to that in Cu$_4$CO$_2$) to Cu(a), which has a positive NBO charge of +0.084. Physisorption via the relatively negative O atom, therefore, is seen to be preferred on the most positively charged metal sites. In both cases, the CO$_2$ molecule remains approximately linear ($\approx$ 178°) and there is little change in the C-O bond lengths. However, it should be noted that the C-O bond which is directly bonded to Cu in Cu$_4$CO$_2$ is slightly elongated (1.17 Å) whereas the other C-O bond is slightly shortened (1.15 Å). On the other hand, in Cu$_6$CO$_2$, both the C-O bond distances in the CO$_2$ moiety remains at 1.16 Å. The O-Cu interaction results in net positive charges (q_{CO2}) of +0.071 and +0.033 on the CO$_2$ molecules in the Cu$_4$CO$_2$ and Cu$_6$CO$_2$ complexes, respectively. The reason for the physisorption of CO$_2$ on Cu$_4$ and Cu$_6$ is probably because both of these clusters have an even number of valence electrons and are closed shell species, with increased stability relative to their odd-electron neighbours, according to the electronic shell model of Knight, Clemenger and co-workers.[93] There is likely to be an appreciable energy barrier to chemisorption in these cases in the gas-phase due to this closed shell arrangement

Unlike the situation on Cu$_4$ and Cu$_6$, CO$_2$ is chemisorbed on the odd-electron (less stable and, therefore, more reactive) Cu$_3$ and Cu$_5$ clusters., CO$_2$ adopts a bent arrangement with two Cu-O bonds. On binding CO$_2$, the Cu$_3$ adopts an approximate equilateral arrangement in which the Cu-Cu edge that binds CO$_2$ is slightly elongated (2.38 Å) compared to other two edges (2.36 Å). CO$_2$ also exhibits a bent geometry on Cu$_5$, bridging the longer Cu(c)-Cu(c) edge. However, in this case the carbon atom lies closer to the Cu atoms binds, along with both oxygen atoms, to the two Cu(c) atoms. In contrast to physisorption, chemisorption involves charge transfer from the metal complex to the π^* molecular orbitals (MOs) of the CO$_2$ molecule. This is supported by the elongation of the C-O bond (1.24 Å on Cu$_3$ and 1.23 Å on Cu$_5$) and the bent CO$_2$ geometry on Cu$_3$ and Cu$_5$. The calculated net NBO charges on the CO$_2$ moiety (q_{CO2}) are large and negative on Cu$_3$ (-0.703) and Cu$_5$ (-0.520) in the gas-phase. It should be noted that, in a combined photoelectron spectroscopy and computational study, Bowen *et al.* have reported the formation of a gas-phase complex between CO$_2$ and a single Cu$^-$ anion, which results in electron transfer and the formation of Cu(CO$_2^-$), where the CO$_2^-$ moiety is bent and bonded to Cu via the carbon atom, with the negative charge delocalised over the π^* framework of the coordinated CO$_2$, corresponding to a formate-like complex .[94] Interestingly, Cu$^-$ only forms the chemisorbed complex with CO$_2$, while Ag$^-$ forms only a C-bound physisorbed complex (with quasi-linear CO$_2$) and Au$^-$ forms both chemisorbed and physisorbed adducts.

(ii) Clusters in water: In contrast to the gas-phase results, the CO$_2$ adsorption free energies are negative in the presence of water. The most stable geometries of the cluster-CO$_2$ complexes also differ between the gas-phase and water. For Cu$_4$, the preferred geometry in water has bent CO$_2$ bridging a Cu(a)-Cu(b) edge, interacting through all of its atoms, as for the gas phase structure of Cu$_5$CO$_2$. CO$_2$ also bridges a different edge of Cu$_5$, Cu(a)-Cu(b), in water, this time bridging through the carbon and only one of the oxygen atoms. This bridging mode is also observed for Cu$_3$CO$_2$ in water. For Cu$_3$-Cu$_5$, there is a more negative net charge on CO$_2$ in water than in the gas-phase, as solvation by a polar solvent (water) stabilises a greater degree of charge separation. Unusually, CO$_2$ does not show any significant interaction with the Cu$_6$ cluster in water, remaining linear and lying parallel to the plane of the Cu$_6$ cluster, at around 3.2 Å, corresponding to

physisorbed CO_2 – which is consistent with the significantly smaller adsorption energy (−0.077 eV). The fact that CO_2 is only physisorbed on Cu_6 perhaps illustrates the fact that this cluster, which has six Cu 3s electrons, has a particularly stable "magic number" electron count (6e), corresponding to a closed shell for the solution of the Schrödinger equation for an electron constrained to a circular disk. In water, chemisorption (on Cu_3, Cu_4 and Cu_5) involves CO_2 bending and cluster-to-CO_2 charge transfer, which is considerably higher in magnitude ($-q_{CO2} > 0.8$) than in the gas-phase, closer to the formate-like structure observed on Cu^- in the gas-phase.[94] As in the gas-phase, the linear physisorbed CO_2 molecule on Cu_6 has a small positive charge (q_{CO2} = +0.01).

Electrocatalytic CO_2RR studies

Next, we investigated the electrochemical pathways for the reduction of CO_2 to various reduction products such as CH_4, CH_3OH and $HCOOH$. Under electrochemical conditions, electrochemical adsorption of CO_2 onto the cluster can compete with the CO_2 adsorption step described in the previous section and it can be considered as the first step in the CO_2RR. Electrochemical adsorption of CO_2 involves a proton-electron pair transfer ($H^+ + e^-$) to CO_2, leading to the formation of the carboxyl species COOH which is adsorbed on the cluster (COOH*). Subsequent electrochemical steps, each of which involves a proton-electron pair transfer, will result in the formation of various electroreduction products such as CO, HCOOH, CH_3OH and CH_4. As in the case of the CO_2* adsorbed cluster complexes, we have found significant stabilization of all the intermediates in water compared to the gas-phase. However, except for a very small number of adsorbed species, the lowest energy geometries for the adsorbed species are the same both in the gas-phase and in water. As the calculations in the gas-phase and in water do not show any significant deviations in CO2RR electroactivity and selectivity as well as in the free energy change patterns and do not provide any additional information, we limit our discussions to the calculations in water only. Moreover, as the electrocatalytic reduction is usually carried out in an aqueous environment, the calculations in the presence of implicit water mimic the experimental conditions more realistically. The results for the gas-phase calculations are given in the supplementary information.

(i)   Electrochemical CO2RR steps on Cu_3 and Cu_4 clusters

First, we will focus on the electrochemical CO2RR steps on Cu_3 and Cu_4 clusters. Figures 2 and 3 show the calculated free energy pathways for the formation of H_2, CO, HCOOH, CH_3OH and CH_4 at zero applied voltage (0 V vs RHE) using the CHE model on Cu_3 and Cu_4, respectively. It can be seen from these free energy profiles that the electrochemical proton-electron reduction pathway $* + CO_2 \rightarrow COOH^* \rightarrow CO^* + H_2O \rightarrow CHO^* \rightarrow CH_2O^* \rightarrow CH_3O^* \rightarrow O^* + CH_4 \rightarrow OH^* \rightarrow * + H_2O$ (Path I) is the lowest energy path for the reduction of CO_2 to CH_4 on both Cu_3 and Cu_4 clusters. CO_2 loses its linearity on electrochemical adsorption to form the carboxyl (COOH*) species on the Cu clusters. The formation of the COOH* species is exergonic on both Cu_3 and Cu_4 clusters, but it is much more favourable on Cu_3 (ΔG = -0.864 eV) than on Cu_4 (ΔG = -0.093 eV). It should be noted that the exergonicity/endergonicty of the formation of the COOH* species shows significant differences on Cu_3 and Cu_4 clusters. Cu_3 has an unpaired electron in its ground electronic state (doublet) and Cu_4 has all of its electrons paired (singlet).

Addition of a second proton-electron pair ($H^+ + e^-$) results in the formation of the CO* species after the elimination of a water molecule. This step is highly exergonic on Cu_4, with a free energy change of -0.697 eV. However, the free energy change for the same step only exhibits low exergonicity on Cu_3 (ΔG = -0.001 eV) compared to Cu_4. The third proton-electron pair transfer hydrogenates the carbon atom of the CO* species, leading to the formation of the CHO* species, which is a strongly endergonic step on Cu_4 with a free energy change of 0.805 eV. This step is the rate-determining free energy step (RDS) on Cu_4. On Cu_3, the hydrogenation of CO* to form CHO* is a weaker endergonic step compared to that on Cu_4 cluster, with a free energy change of 0.102 eV.

Figure 2: Free energy changes (ΔG; solvent-corrected, eV) calculated for the electrochemical pathways for the reduction of CO_2 on the Cu_3 cluster, employing the CHE model. The lowest energy geometries for the various adsorbed species are shown in the lower panel.

The next (H⁺ + e⁻) pair transfer hydrogenates CHO* to formaldehyde (CH_2O*). On Cu_3, this is an mildly exergonic step (ΔG = -0.252 eV). In contrast, on Cu_4, the formation of CH_2O* from CHO* is highly exergonic with a free energy change of -0.639 eV. The fifth proton-electron pair transfer leads to the hydrogenation of CH_2O* to the adsorbed methoxy species (CH_3O*). Even though this step is exergonic for both the Cu_3 and Cu_4 clusters, the exergonicity of the reaction is larger on Cu_3 (ΔG = -1.251 eV) compared to Cu_4 (ΔG = -0.398 eV).

The sixth (H⁺ + e⁻) pair transfer adds another hydrogen to the carbon atom, followed by the elimination of CH_4 leaving an adsorbed O* species. Whereas this reaction step is a thermodynamically unfavourable endergonic process on Cu_3 (ΔG = 0.370 eV), it is a thermodynamically highly favourable exergonic process on Cu_4 (ΔG = -1.316 eV). The seventh (H⁺ + e⁻) pair transfer leads to the formation of an OH* species. This is a highly exergonic step on Cu_3, with a free energy change of -1.107 eV. The eighth proton-electron transfer hydrogenates the oxygen centre of the OH* species and regenerates the free Cu_3 cluster following the release

of a water molecule. However, the last-step is highly endergonic, with a free energy difference of 0.655 eV, and is the RDS on Cu_3. This step will, most likely, not occur experimentally under a zero applied potential.

For Cu_4, the formation of the OH* by the seventh $(H^+ + e^-)$ transfer is mildly exergonic (ΔG = -0.011 eV). In contrast to the Cu_3 cluster, where the final step is the RDS, on Cu_4, the elimination of H_2O and the regeneration of the free Cu_4 cluster surface occurs with almost zero energetic cost. Instead, the RDS on the Cu_4 cluster is the formation of CHO* from CO*, which requires a free energy change of 0.805 eV. To overcome the most endergonic RDS step on Cu_3 (removing OH* as water), to make it exergonic, requires the application of a limiting potential (U_L) of 0.655 V. On Cu_4, the limiting potential is 0.805 V to make the RDS (CO*→CHO*) exergonic.

We have also investigated the alternative pathway (Path II): * + CO_2 → COOH* → C(OH)$_2$* → COH* + H_2O→ C* + H_2O→ CH* → CH$_2$* → CH$_3$* → CH$_4$ + * for the 8-electron reduction of CO_2 to methane. This alternative pathway starts with the formation of C(OH)$_2$* from COOH*. Figure 2 shows that the electrochemical step COOH*→ C(OH)$_2$* is a thermodynamically uphill process on Cu_3 and Cu_4. However, the endergonicity is quite large on Cu_3 (1.836 eV) compared to that on Cu_4 (0.941 eV). The next $(H^+ + e^-)$ pair transfer to C(OH)$_2$* forms the COH* species by eliminating a water molecule with an exergonic free energy of -0.304 eV on Cu_3. On Cu_4, the same step exhibits high endergonicity (0.674 eV). It is also possible that the third $(H^+ + e^-)$ pair transfer can form COH* by direct hydrogenation of CO*. However, this is one of the most highly endergonic reaction steps, with free energy changes of Cu_3 (1.533 eV) and Cu_4 (2.312 eV) and is, therefore, not feasible. Further proton-electron transfers lead to the formation of C*, CH*, CH$_2$*, CH$_3$* and finally the release of CH$_4$ from the Cu_3 cluster. We have found in general that there is a reversal of exergonicity or endergonicity of these reaction steps on Cu_3 and Cu_4. Overall, it is quite unlikely that the reaction proceeds through this alternative pathway, as the formation of the intermediate C(OH)$_2$* has to compete with the thermodynamically favoured exergonic step COOH* → CO* + H_2O.

Other alternative pathways (Path III): * + CO_2 → COOH* → CO* + H_2O→ CHO* → CHOH* → CH*+ H_2O → CH$_2$* → CH$_3$* → CH$_4$ + * and Path (IV): * + CO_2 → COOH* → CO* + H_2O→ CHO* → CH$_2$O* → CH$_2$OH* → CH$_2$* + H_2O → CH$_3$* → CH$_4$ + * were also investigated for CH$_4$ formation. Even though, the fourth $(H^+ + e^-)$ pair can either form CH$_2$O* or CHOH* species by hydrogenating the carbon or oxygen centres of the CHO group, respectively, the formation of CH$_2$O* is thermodynamically favourable on both clusters. While the formation of CHOH* is an endergonic process on the Cu_3 and Cu_4 clusters, the endergonicity of this step is larger on Cu_3 than on Cu_4. In a similar way, though the fifth proton-electron transfer can form CH$_3$O* or CH$_2$OH* by hydrogenating the carbon or oxygen centres of the CH$_2$O* species, thermodynamically the formation of CH$_3$O* is favoured on both the Cu_3 and Cu_4 clusters. From a thermodynamic point of view, reaction pathways III and IV are less favoured than pathway I as the electrochemical step CHO* → CH$_2$O* is preferred over CHO* → CHOH* and CH$_2$O*→ CH$_3$O* step is preferred over CH$_2$O* → CH$_2$OH*.

Next, we discuss the formation of the 6-electron reduction product methanol (another desired CO_2 reduction product) on Cu_3 and Cu_4 clusters. The three lowest energy reaction pathways to methanol formation are: (i) * + CO_2 → COOH* → CO* + H_2O → CHO* → CH$_2$O* → CH$_3$O* → CH$_3$OH + * (Path V); (ii) * + CO_2 → COOH* → CO* + H_2O → CHO* → CHOH* → CH$_2$OH* → CH$_3$OH + * (Path VI); and (iii) * + CO_2 → COOH* → CO* + H_2O → CHO* → CH$_2$O* → CH$_2$OH* → CH$_3$OH + * (Path VII). Methanol formation on Cu clusters should compete with the formation of methane. The sixth $(H^+ + e^-)$ pair transfer to CH$_3$O* can lead to release of CH$_3$OH from the clusters (path V). However, the formation of CH$_3$OH is in competition with the formation of CH$_4$ from the CH$_3$O* intermediate via Path I. Methanol formation from CH$_3$O* is a highly endergonic step and is the RDS on Cu_3 clusters, with a free energy change of 1.256 eV corresponding to a limiting potential of 1.256 V. From Figure 2, it is clear that the formation of CH$_4$ is thermodynamically more favourable on Cu_3 than the formation of CH$_3$OH, even though both CH$_4$ and CH$_3$OH formation are endergonic processes on the Cu_3 cluster. In a similar way, the formation of CH$_4$ is thermodynamically highly favourable on Cu_4 than the formation of CH$_3$OH. The electrochemical step CH$_3$O* → O* + CH$_4$ is significantly preferred over CH$_3$O* → CH$_3$OH by 0.886

11

eV and 1.328 eV on Cu_3 and Cu_4, respectively. Again, it is interesting to note the switch between exergonicity and endergonicity of the $CH_3O^* \rightarrow O^* + CH_4$ and $CH_3O^* \rightarrow CH_3OH^*$ reactions when comparing the Cu_3 and Cu_4 clusters.
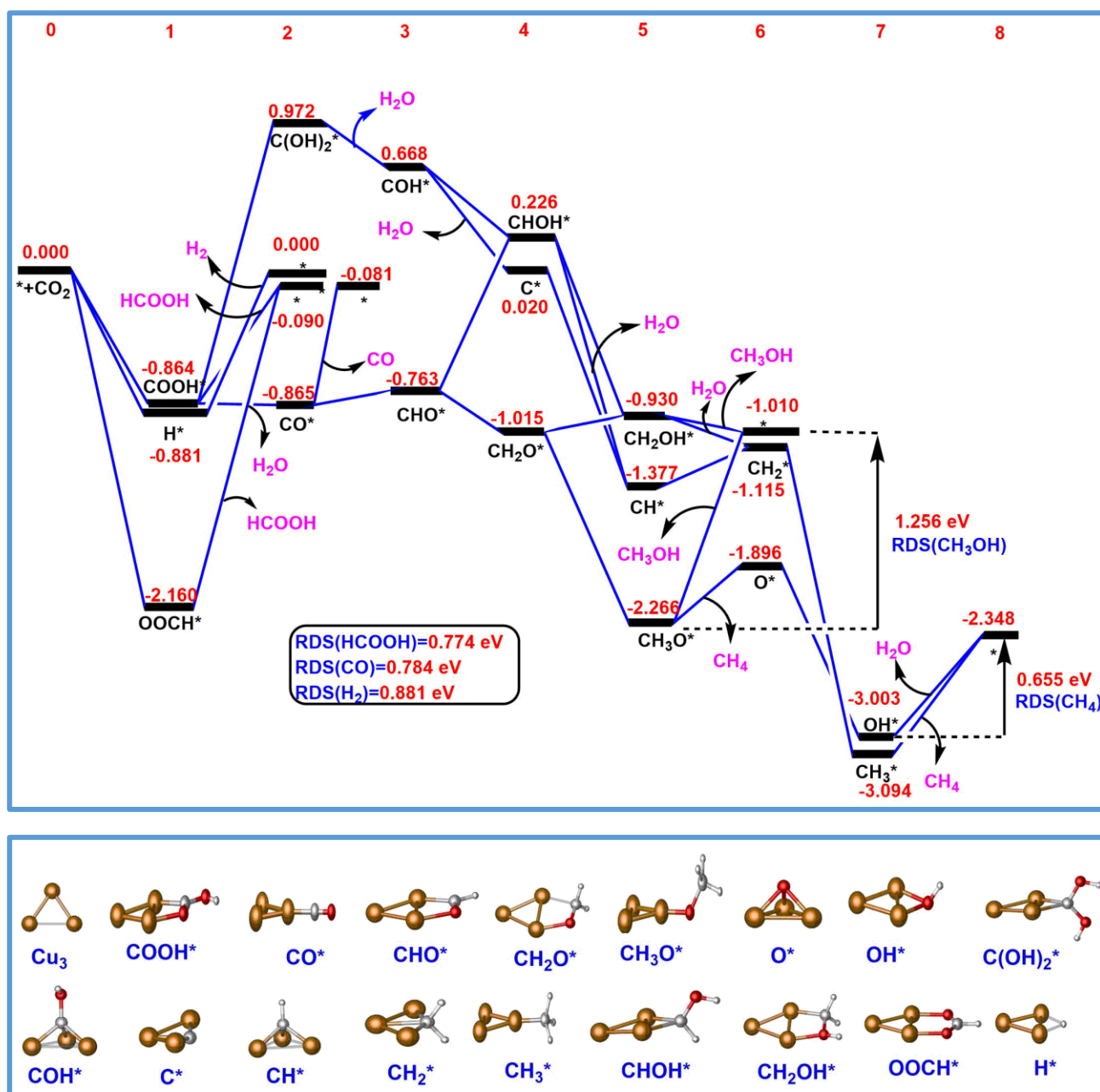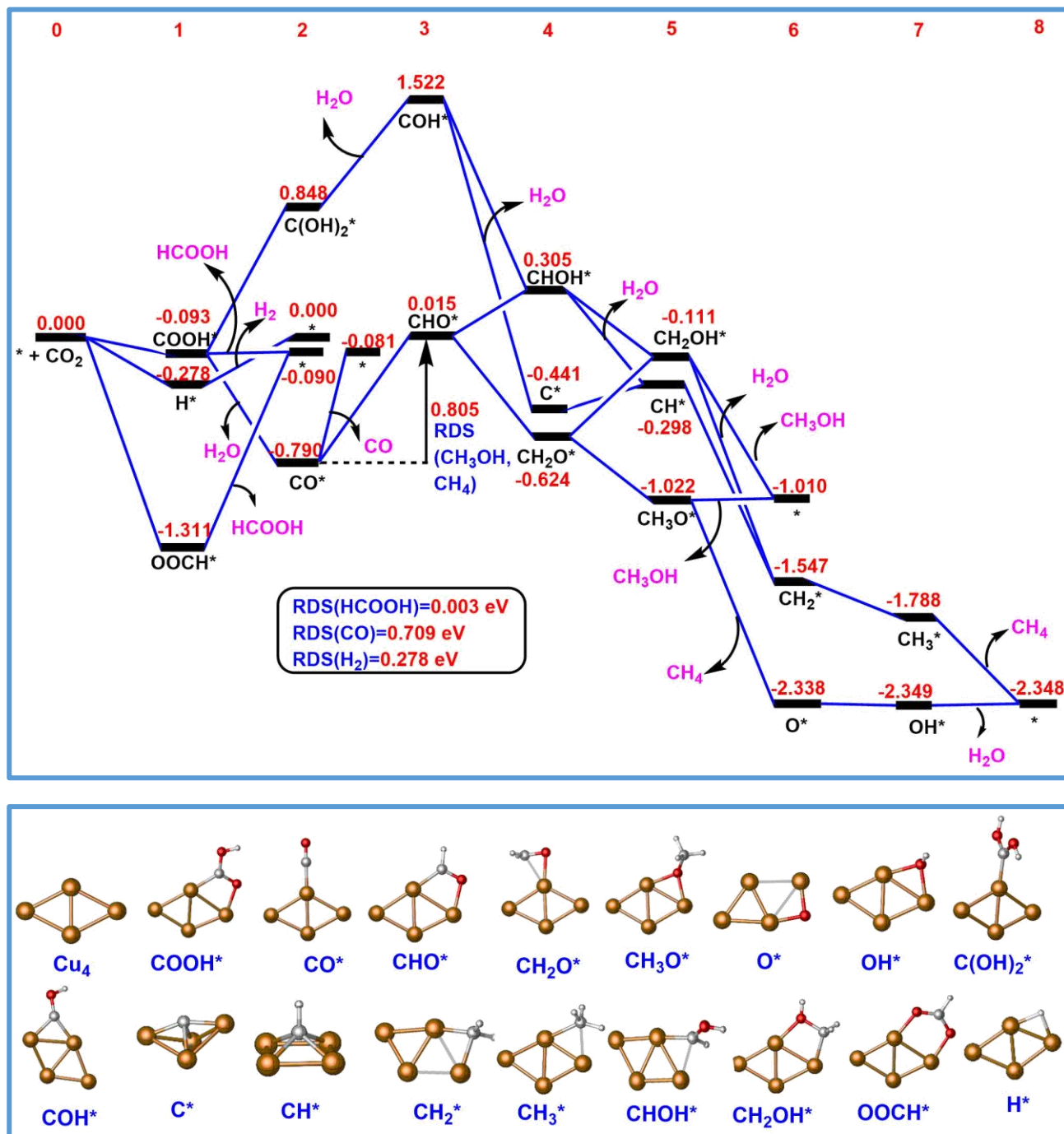

Figure 3: Free energy changes (ΔG; solvent-corrected, eV) calculated for the electrochemical pathways for the reduction of CO_2 on the Cu_4 cluster, employing the CHE model. The lowest energy geometries for the various adsorbed species are shown in the lower panel.

The methanol formation pathways VI and VII depend on the favourability of the formation of CHOH* and CH_2OH^* adsorbates on Cu clusters and also on the thermodynamic preference for CH_4 formation via paths III and IV. As mentioned earlier, the formation of CHOH* from CHO* and CH_2OH^* from CH_2O^* should compete with the formation of the thermodynamically more favourable CH_2O^* and CH_3O^* species in the fourth and fifth electrochemical steps. Moreover, CHOH* $\rightarrow$ CH* + H_2O (Path III) is preferred over CHOH* $\rightarrow$ CH_2OH^* (path VI) and $CH_2OH^* \rightarrow CH_2^* + H_2O$ (path IV) is preferred over $CH_2OH^* \rightarrow CH_3OH + *$ (path VII) on both Cu_3

and Cu_4 clusters and leads to the exclusive formation of CH_4. The unfavorability in the formation of $CHOH^*$, CH_2OH^* and CH_3OH from CHO^*, CH_2O^* and CH_3O^*, respectively and the thermodynamic preference for the methane formation pathways $CHOH^* \rightarrow CH^* + H_2O$ and $CH_2OH^* \rightarrow CH_2^* + H_2O$ over methanol formation pathways $CHOH^* \rightarrow CH_2OH^*$ and $CH_2OH^* \rightarrow CH_3OH + *$ indicates the exclusive formation of CH_4 as the major product and is in line with the absence of CH_3OH production on experimental electrocatalytic studies on the Cu surface.

Considering all the different CH_3OH formation pathways (Paths V-VII), the formation of CH_3OH if any, proceeds via the pathway V. The limiting potential for the opening of the CH_3OH formation pathway on the Cu_3 cluster is 1.256 V. On Cu_4, the limiting potential to be applied for the formation of CH_3OH is 0.805 V. These values are identical to those for CH_4 formation since the RDS is $CO^* \rightarrow CHO$ for both pathways on Cu_4.

The formation of CH_4 and CH_3OH on Cu clusters has to compete with other side reactions, mainly the 2-electron reduction pathways to form HCOOH, CO and H_2. Formic acid can be formed either via (i) $* + CO_2 \rightarrow COOH^* \rightarrow HCOOH + *$ (Path VIII) or (ii) $* + CO_2 \rightarrow OOCH^* \rightarrow HCOOH + *$ (Path IX). Even though the formation of the formate species ($OOCH^*$) species in the first ($H^+ + e^-$) pair transfer is a highly favourable downhill step on both Cu_3 and Cu_4 clusters, the release of HCOOH from the cluster surface by the transfer of the second ($H^+ + e^-$) pair is a highly unfavourable uphill process, so it is unlikely that HCOOH formation proceeds via the $OOCH^*$ pathway. The formation of $COOH^*$ is highly exergonic on Cu_3, whilst the next electrochemical proton-electron transfer step (leading to the release of HCOOH) is endergonic with a free energy change of 0.774 eV and is the RDS for the opening of the HCOOH formation pathway on Cu_3. The exergonicity and endergonicity of these steps are again reversed on the Cu_4 cluster. The formation of $COOH^*$ has an exergonic free energy change of -0.093 eV and the release of free HCOOH in the second ($H^+ + e^-$) transfer step just requires 0.003 eV. This shows that the formation of HCOOH is a spontaneous step in water and, therefore, can proceed without an applied voltage.

The carboxyl species $COOH^*$ can also form CO by eliminating a water molecule after the second ($H^+ + e^-$) transfer step and this can compete with the formation of HCOOH. The elimination of water leads to adsorbed CO^* species which then releases the free CO, in a two-step process $COOH^* \rightarrow CO^* + H_2O \rightarrow CO + *$ (Path X). Desorption of CO from the cluster to form free CO ($CO^* \rightarrow CO + *$) is a non-electrochemical step as it does not involve any ($H^+ + e^-$) pair transfer and is highly endergonic on both Cu_3 and Cu_4. On the Cu_3 cluster, the formation of the adsorbed CO^* species from the carboxyl species $COOH^*$ does not involve any significant free energy change. However, desorption of the adsorbed CO^* is highly endergonic on Cu_3, with a free energy change of 0.784 eV and is the RDS for the formation of CO. On Cu_3, the formation of HCOOH and CO are almost equally probable, with a free energy difference of only 0.010 eV.

In contrast to Cu_3, the free energy profile for the Cu_4 cluster (Figure 3) shows that the formation of CO^* from $COOH^*$ is thermodynamically highly preferred over the formation of HCOOH. The electrochemical step $COOH^* \rightarrow CO^* + H_2O$ is associated with the exergonic free energy change of -0.697 eV whereas the $COOH^* \rightarrow HCOOH + *$ electrochemical step is weakly endergonic (0.003 eV). However, the desorption of CO^* is a highly endergonic step, with a free energy change of 0.709 eV, which is comparable to the CO desorption free energies of 0.784 eV on Cu_3. This shows that the free energies for the CO desorption step (which does not involve proton-electron pair transfer) on Cu_3 and Cu_4 are not significantly different. Another important aspect we should consider is that the formation of CH_4 and CH_3OH is only feasible if the adsorbed CO^* species remains on the surface for further reduction. The viability of these higher reduction products depends on whether the adsorbed species prefer to form CHO^* in the next electrochemical transfer step or to desorb from the cluster. On the Cu_3 cluster, the formation of CHO^* ($CO^* \rightarrow CHO^*$) is preferred over the desorption step by 0.682 eV. In contrast, on Cu_4 the desorption of adsorbed CO^* is favoured over further electroreduction to CHO^* by 0.096 eV. In other words, the feasibility and selectivity of forming the higher reduction products methane and methanol are more favoured on the Cu_3 cluster than on the Cu_4 cluster as the formation of CHO^* from CO^* is more favourable on Cu_3 compared to desorption of CO from the cluster.

We have also investigated selectivity for the hydrogen evolution reaction (HER), which is a competing side reaction to CO$_2$RR. The (H$^+$ + e$^-$) pair can adsorb on the cluster surface as H*, which is a highly favourable exergonic step on Cu$_3$, with a reaction free energy change of -0.881 eV. Although this step is also exergonic on the Cu$_4$ cluster, in line with our previous observations, the exergonicity is considerably smaller on Cu$_4$ (-0.278 eV). The second (H$^+$ + e$^-$) pair transfer to the adsorbed H* species triggers the release of the H$_2$ molecule from the cluster. This step is endergonic by 0.881 eV on Cu$_3$ and is the RDS on Cu$_3$. Conversely, the release of H$_2$ from Cu$_4$ is a less endergonic by 0.278 eV. One of the major challenges in CO$_2$ electroreduction is to supress the competing HER reaction. Our findings show that hydrogen evolution is more hindered on the Cu$_3$ cluster because there is a higher limiting potential for H$_2$ release on Cu$_3$ than on Cu$_4$.

(ii)   Comparison of exergonicity/endergonicity of CO2RR steps on Cu$_3$ and Cu$_4$ clusters

We have identified a general trend in the exergonicity and/or endergonicity of each step with the spin state of the cluster-adsorbate intermediate complex. We have plotted the free energy changes for various electrochemical steps on Cu$_3$ and Cu$_4$ that involve an odd number of (H$^+$ + e$^-$) pair transfers (steps a-k) and an even number of (H$^+$ + e$^-$) pair transfers (steps l-aa) separately in Figure 4. See Table 2 for a description of all the steps and the spin state of the adsorbate on clusters with odd numbers of electrons (Cu$_3$ and Cu$_5$) and even numbers of electrons (Cu$_4$ and Cu$_6$).

Table 2: The total number of (H$^+$ + e$^-$) pair transfer steps to CO$_2$ for the formation of cluster-adsorbate intermediates and the spin state (S = singlet; D = doublet) of the intermediate for electrochemical steps (a-aa), comparing odd-electron clusters (Cu$_3$ and Cu$_5$) and even-electron (Cu$_4$ and Cu$_6$) clusters.

Electrochemical Step		Total number of (H$^+$ + e$^-$) pair transfer steps to CO$_2$	Spin state of the adsorbate on	
			Cu$_3$, Cu$_5$	Cu$_4$, Cu$_6$
Odd number of (H$^+$ + e$^-$) pair transfer steps				
a	* + CO2 → COOH*	1	S	D
b	CO* → CHO	3	S	D
c	CH$_2$O* → CH$_3$O*	5	S	D
d	O* → OH*	7	S	D
e	C(OH)$_2$* → COH*+H$_2$O	3	S	D
f	C* → CH*	5	S	D
g	CH$_2$* → CH3*	7	S	D
h	CHOH* → CH$_2$OH*	5	S	D
i	CH$_2$O* → CH$_2$OH*	5	S	D
j	* + CO$_2$ → OOCH*	1	S	D
k	*→ H*	1	S	D
Even number of (H$^+$ + e$^-$) pair transfer steps				
l	COOH* → CO* + H$_2$O	2	D	S
m	CHO* → CH$_2$O*	4	D	S
n	CH$_3$O* → O* + CH$_4$	6	D	S
o	OH* → * + H$_2$O	8	D	S
p	COOH* → C(OH)$_2$*	2	D	S
q	COH* → C*	4	D	S
r	CH* → CH$_2$*	6	D	S
s	CH$_3$* → * +CH$_4$	8	D	S
t	CH$_3$O* → * + CH$_3$OH	6	D	S
u	CHO* → CHOH*	4	D	S
v	CH$_2$OH* → * + CH$_3$OH*	6	D	S
w	COOH* → * + HCOOH	2	D	S
x	OOCH* → * + HCOOH	2	D	S
y	COOH*→ * + CO +H$_2$O	2	D	S
z	H* → * + H$_2$	2	D	S
aa	COH* → CHOH*	4	D	S

Figure 4 clearly shows that the exergonicity/endergonicity of each electrochemical step in the formation of CH_4 shows a significant difference for the Cu_3 and Cu_4 clusters. On Cu_3, the reaction steps $* + CO_2 \rightarrow COOH*$ (step a in Figure 4), $CH_2O* \rightarrow CH_3O*$ (c) and $O* \rightarrow OH*$ (d) are exergonic, with reaction free energies of -0.864 eV, -1.251 eV and -1.106 eV. These same reaction steps are mildly exergonic on the Cu_4 cluster, with free energies of -0.093 eV, -0.398 eV and -0.011 eV. Although the electrochemical step $CO* \rightarrow CHO*$ (b) is endergonic on both Cu_3 and Cu_4, the degree of endergonicity is much larger on Cu_4 (0.805 eV) compared to Cu_3 (0.102 eV) and is the RDS on the Cu_4 cluster for the eight-electron reduction to CH_4, but not on the Cu_3 cluster. It should be noted that the intermediates COOH*, CHO*, CH_3O*, and OH* are formed on the first, third, fifth and seventh electrochemical ($H^+ + e^-$) pair transfers (i.e. an odd total number of electrons transferred) and (because of the odd number of electrons of the Cu_3 cluster) give rise to singlet spin ground states for the Cu_3-adsorbate complex. In contrast, on the (even-electron) Cu_4 cluster, these intermediate complexes have doublet ground spin states.

The reaction steps $COOH* \rightarrow CO* + H_2O$ (l), $CHO* \rightarrow CH_2O*$ (m), $CH_3O* \rightarrow * + CH_4$ (n) and $OH* \rightarrow * + H_2O$ (o) are predominantly endergonic or mildly exergonic on the Cu_3 cluster, with reaction free energies of -0.001 eV, -0.252 eV, $+0.370$ eV and $+0.655$ eV. These same steps are more favoured, being more strongly exergonic or mildly endergonic on Cu_4, with respective reaction free energies of -0.697 eV, -0.656 eV, -1.316 eV and $+0.002$ eV. Again, it should be noted that these reaction steps involve the second, fourth, sixth and eighth ($H^+ + e^-$) pair transfers (*i.e.* even numbers of electrons transferred) and the cluster-adsorbate intermediate complexes have doublet spin ground states on the (odd-electron) Cu_3 cluster and singlet states on the (even-electron) Cu_4.

We have also noticed that there is a significant difference in reaction step endergonicities on the Cu_3 and Cu_4 clusters for the alternative CH_4 pathways. For example, on Cu_3 the free energy change for the reaction step $COOH* \rightarrow C(OH)_2*$ (p) is more endergonic (+1.836 eV) than on Cu_4 (+0.941 eV). The reverse is found for the reaction $C(OH)_2* \rightarrow COH* + H_2O$ (e), which is more endergonic on Cu_4 (+0.674 eV) than on Cu_3 where it is exergonic (-0.303 eV). It should be noted that the species $C(OH)_2*$ and COH* are formed in the second and third electrochemical proton-electron transfer steps, respectively, and correspond to doublet and singlet cluster-adsorbate complexes on Cu_3, while they are singlet and doublet complexes on Cu_4.

We have also found similar alterations in the exergonicity/endergonicity for other species. On the Cu_3 cluster, the reaction steps $COH* \rightarrow C* + H_2O$ (q), $CH* \rightarrow CH_2$ (r) and $CH_3 \rightarrow * + CH_4$ (s), which involve the fourth, sixth and eighth ($H^+ + e^-$) pair transfers, are either exergonic or endergonic, with reaction free energy changes of -0.649 eV, $+0.261$ eV and $+0.747$ eV. The same reaction steps are more highly exergonic on the Cu_4 cluster, with reaction free energies of -1.963 eV, -1.249 eV and -0.560 eV. Furthermore, on Cu_3 the fifth and seventh reaction steps $C* \rightarrow CH*$ (f) and $CH_2* \rightarrow CH_3*$ (g) are highly exergonic, with free energy differences of -1.396 eV and -1.979 eV. Conversely, on Cu_4 these steps are less thermodynamically favoured, being only mildly exergonic or endergonic (+0.144 eV and -0.241 eV). Similar changes on the extent of exergonicity and endergonicity are clearly visible for other electrochemical steps that lead to CH_3OH and two-electron reduction products.
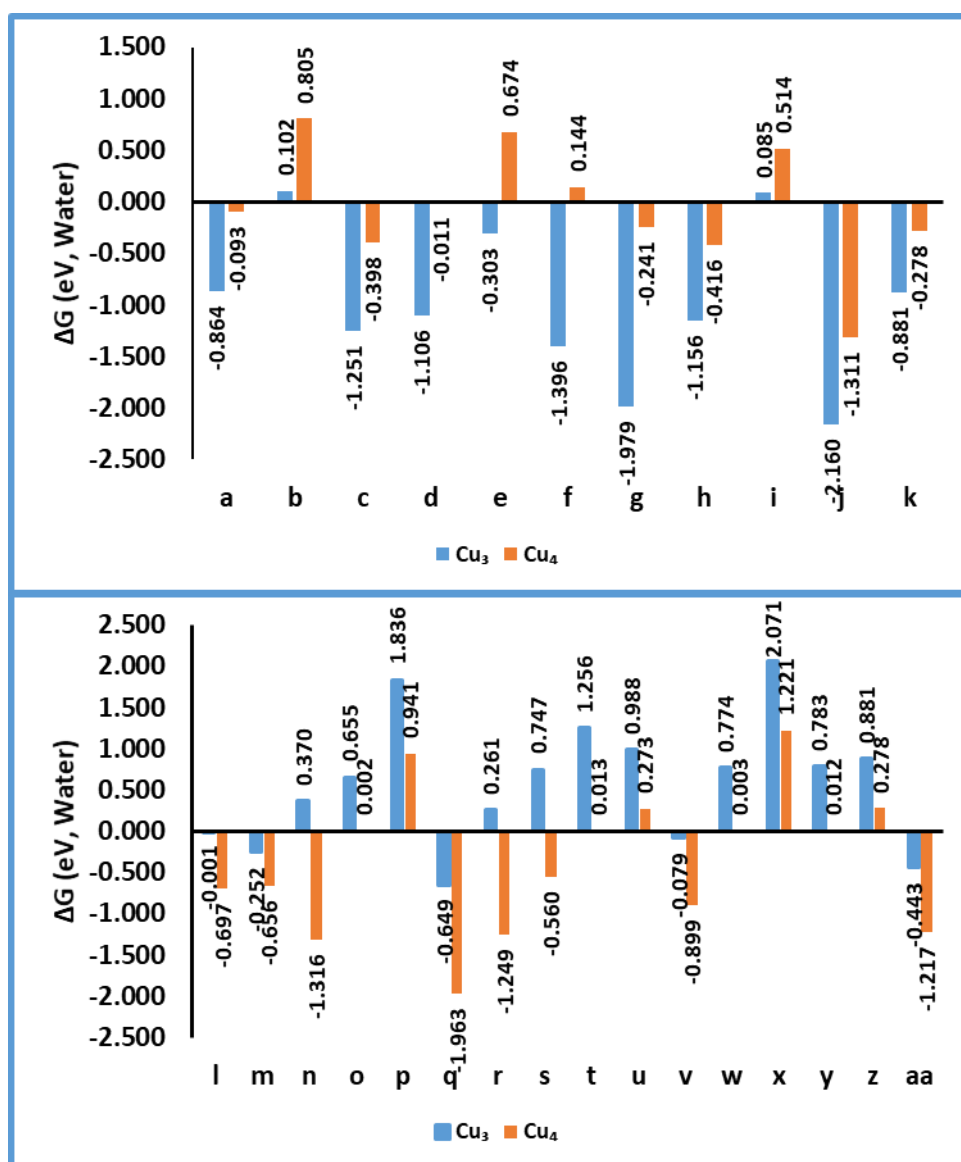
Figure 4: Free energy changes (eV) for the various electrochemical steps that involve odd (a-k) (top) or even total number (l-aa) (bottom) of (H$^+$ + e$^-$) pair transfers on Cu$_3$ and Cu$_4$ clusters. This graph shows the ender/exergonicity of each electrochemical step on Cu$_3$ and Cu$_4$. See Table 2 for a description of each step and the spin states of the various cluster-adsorbate intermediates on the Cu$_3$ and Cu$_4$ clusters.

To make it more clear regarding the direct relationship between the spin state of the cluster-adsorbate species and the free energy changes for each electrochemical step, we have plotted the exergonicity or endergonicity of each electrochemical (H$^+$ + e$^-$) transfer step on the Cu$_4$ cluster with respect to that on Cu$_3$ i.e. the difference of the free energy changes in each electrochemical proton-electron pair transfer step (ΔΔG = ΔG(Cu$_4$) − ΔG(Cu$_3$)) in Figure 5. This clearly shows that the endergonicities of the first, third, fifth and seventh electrochemical (H$^+$ + e$^-$) steps for the production of CH$_4$ (* + CO$_2$ → COOH* (a), CO* → CHO* (b), CH$_2$O* → CH$_3$O* (c) and O* →OH* (d)) are considerably larger on Cu$_4$, whereas the second, fourth sixth and eighth electrochemical steps (COOH* → CO* + H$_2$O (l), CHO* → CH$_2$O* (m), CH$_3$O* → CH$_4$ + * (n), OH* → H$_2$O + *(o)) are more highly exergonic on Cu$_4$ compared with the same steps on Cu$_3$. The steps in the alternative CH$_4$ pathway via C(OH)$_2$* also exhibit the same trend. The endergonicity of the steps C(OH)$_2$* → COH* +H$_2$O (e), C* → CH* (f), and CH$_2$* → CH3* (g) and the exergonicity of the steps COOH* → C(OH)$_2$* (p) , COH* → C* (q), CH* → CH$_2$* (r) and CH$_3$* → * + CH$_4$ (s) are significantly larger on Cu$_4$ than on Cu$_3$. Similarly, the electrochemical steps for CH$_3$OH production that involve the fifth proton-electron pair transfer (CHOH* → CH$_2$OH* (h) and CH$_2$O* → CH$_2$OH* (i)) are significantly more endergonic on Cu$_4$ than Cu$_3$. Conversely, the

steps that involve an odd number of (H$^+$ + e$^-$) pair transfers (CH$_3$O* → * + CH$_3$OH (t), CHO*→ CHOH* (u), CH$_2$OH* → * + CH$_3$OH (v) and COH* → CHOH* (aa)) are more exergonic on Cu$_4$. The HCOOH, CO and H$_2$ formation pathways (steps a, j, k, l, w, x, y and z) show similar changes in their exergonicity and endergonicity on Cu$_3$ and Cu$_4$ clusters.
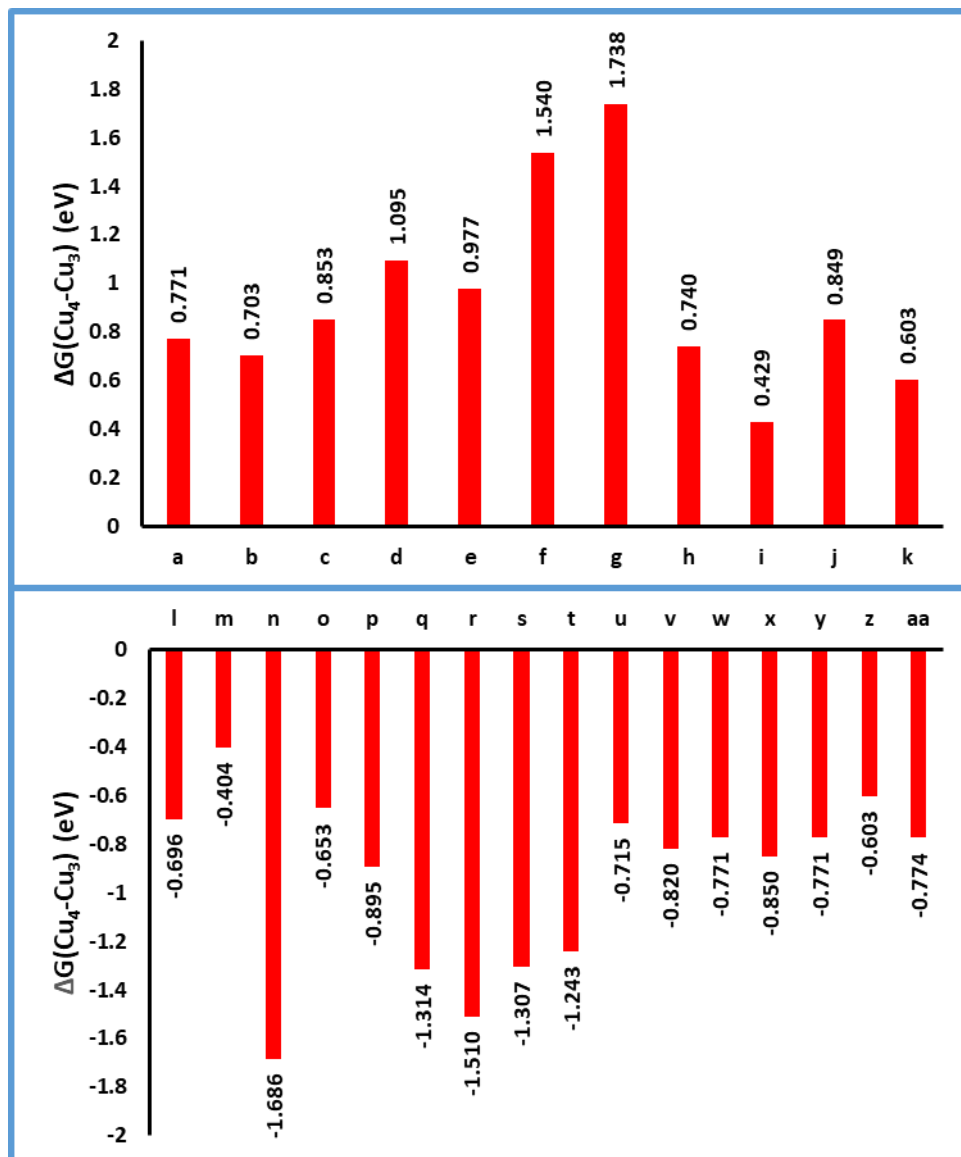

Figure 5: Ender-/exergonicity for the various electrochemical steps that involve odd (top) or even total number (bottom) of (H$^+$ + e$^-$) pair transfers on the Cu$_4$ cluster relative to the ender/exergonicity on the Cu$_3$ cluster; *i.e.* the difference between the free energy change on the Cu$_4$ and Cu$_3$ clusters for each electrochemical step in water (ΔΔG=ΔG(Cu$_4$)-ΔG(Cu$_3$))

In general, we have found a striking relationship between exer/endergonicity of the electrochemical proton-electron transfer step and the spin state. Electrochemical (H$^+$ + e$^-$) transfer to a doublet spin state cluster-adsorbate complex (having a single unpaired electron) leads to the formation of a singlet intermediate species (having no unpaired electrons): this step is a thermodynamically favourable exergonic process. However, electrochemical (H$^+$ + e$^-$) transfer to a singlet spin state cluster-adsorbate complex results in the formation of a doublet intermediate species: this step is a thermodynamically unfavourable endergonic process.

(iii)   CO₂RR on Cu₅ and Cu₆ clusters

The free energy profiles for the electrochemical pathways for the reduction of CO_2 to CH_4 on Cu_5 and Cu_6 clusters are shown in Figures 6 and 7, respectively. We have found striking similarity between the free energy pathways for the Cu_3 and Cu_5 clusters, which both possess doublet spin ground states (with one unpaired electron) and between the Cu_4 and Cu_6 clusters, which possess singlet spin ground states (with no unpaired electrons).

The formation of CH_4 follows the same lowest energy route * + CO_2 → COOH* → CO* + H_2O → CHO* → CH_2O* → CH_3O* → O* + CH_4 → OH* → * + H_2O (Path I) on both Cu_5 and Cu_6 clusters as in the case of the Cu_3 and Cu_4 clusters. As for Cu_3 and Cu_4, the alternative pathway via C(OH)₂* is unfavoured. The free energy changes for various proton-electron transfer steps on Cu_5 are quite similar to those on Cu_3. As observed for Cu_3, the formation of the singlet cluster-adsorbate intermediates COOH*, CH_3O* and OH* on the first, fifth and seventh electrochemical (H^+ + e^-) pair transfer steps from the preceding doublet species are the most exergonic electrochemical steps on Cu_5. Similarly, the second, sixth and eighth electrochemical steps COOH → CO*, CH_3O* → O* + CH_4 and OH* → * + H_2O (involving a change from singlet to doublet spin states) are endergonic. Unlike the formation of the aforementioned singlet species with large exergonic free energy changes, the third electrochemical step CO* → CHO* is only mildly exergonic (-0.156 eV). This can be attributed to the energetic requirement for the reorganization of the 3D trigonal bipyramidal Cu_5 core of the CO* species back to the planar "W-shaped" geometry of the CHO* species. This results in the high free energy of the CHO* species in the potential energy surface and is also the reason for the mildly exergonic free energy change of -0.057 eV for the fourth CHO* → CH_2O* electrochemical step, even though this is a singlet-to-doublet step. As in the case of the Cu_3 cluster, the RDS on Cu_5 is the removal of the adsorbed O* species from the cluster as H_2O in the eighth electrochemical step, which has an endergonic free energy change of 1.062 eV.

Similarly, the various electrochemical pathways and the free energy changes for the formation of methanol on Cu_5 are very similar to those on Cu_3. As for Cu_3 and Cu_4, the lowest energy pathway for CH_3OH production is * + CO_2 → COOH* → CO* + H_2O → CHO* → CH_2O* → CH_3O* → * + CH_3OH (Path V). The electrochemical step CH_3O* → CH_3OH + * is found to be the rate-limiting electrochemical step on Cu_5, with a high endergonic free energy requirement of 1.075 eV. These rate-limiting free energies are comparable to the high endergonic limiting free energy 1.256 eV on Cu_3. It should be noted that, as on the Cu_3 and Cu_4 clusters, the formation of CH_3OH via the CHO* → CHOH and CH_2O* → CH_2OH* steps are not feasible, as the competing steps CHO* → CH_2O* and CH_2O* → CH_3O* are more thermodynamically favoured. As for Cu_3 and Cu_4, the preference for the formation of CH_4 over CH_3OH in the sixth (H^+ + e^-) pair transfer step is evident from the free energy profiles. Although the lowest energy pathways to CH_3OH are similar on the Cu_3, Cu_4 and Cu_5 clusters, we have found that the endergonicity and exergonicity of the various steps show greater similarity between Cu_3 and Cu_5.

The two-electron reduction steps for the generation of HCOOH, CO and H_2 again show the greatest similarity between Cu_3 and Cu_5. On Cu_5, the formation of the carboxyl species COOH* is a thermodynamically favoured downhill process. The limiting free energy change for the release of HCOOH is 1.015 eV on Cu_5. The formation of CO proceeds through the two-step process COOH* → CO* + H_2O → CO + * on the Cu_5 cluster. The RDS is the non-electrochemical desorption step (CO* → CO + *) with a free energy change of 0.737 eV. However, the adsorbed CO* preferentially undergoes further reduction to CHO*, as this is thermodynamically favoured downhill step over the desorption step. Hydrogen evolution on Cu_5 has a very high rate-limiting free energy of 1.251 eV to release the adsorbed H* species as H_2. As the free energy requirement for the release of H_2 is quite large, it is expected that HER does not compete significantly with the formation of higher reduction products methane and methanol as in the case of Cu_3.
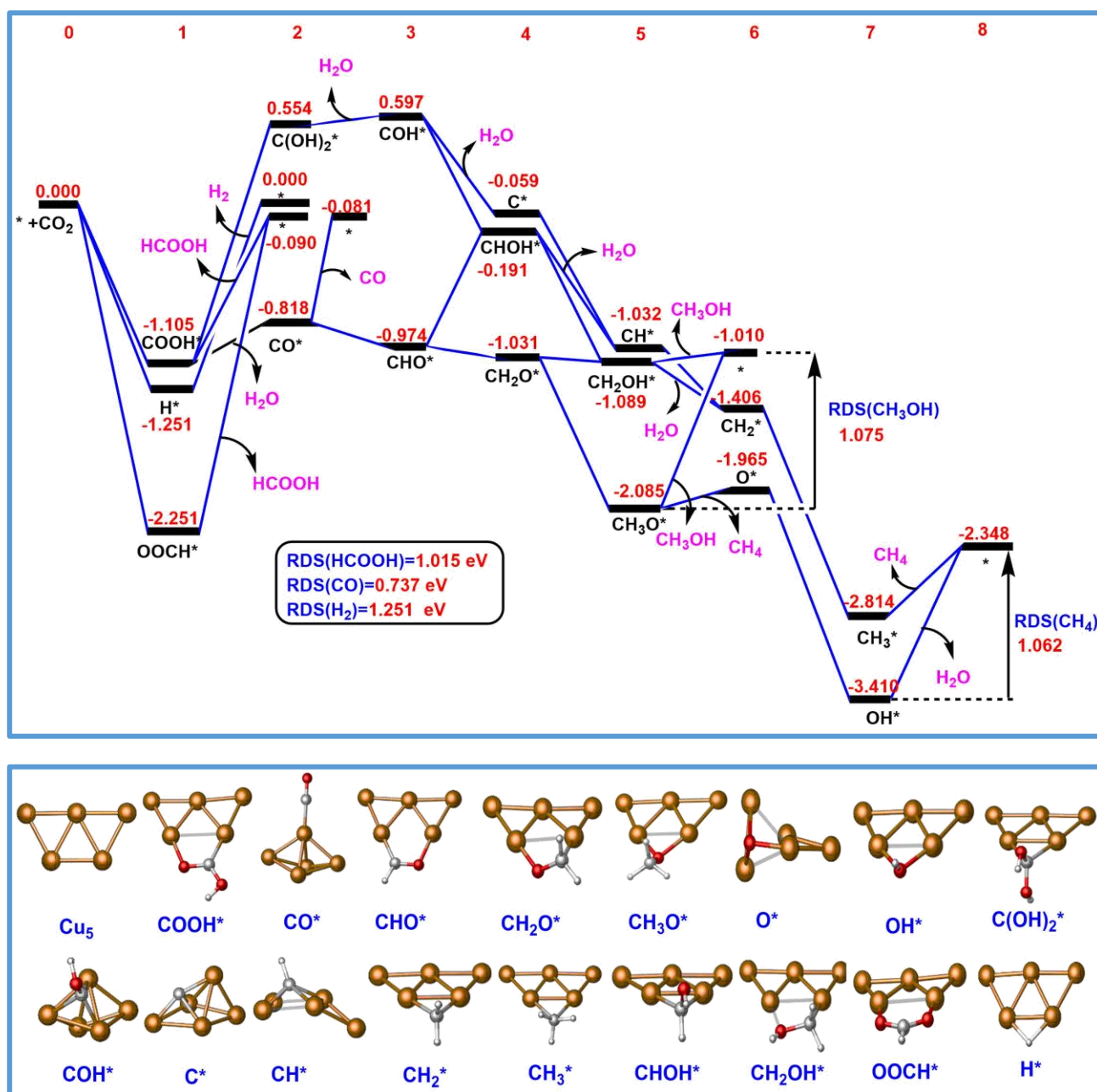
Figure 6: Free energy changes (ΔG; solvent-corrected, eV) calculated for the electrochemical pathways for the reduction of CO_2 on the Cu_5 cluster, employing the CHE model. The lowest energy geometries for the various adsorbed species are shown in the lower panel.

The pattern of free energy changes for various electrochemical pathways on the Cu_6 cluster are very similar to those on the Cu_4 cluster. The lowest energy pathways for the production of CH_4 and CH_3OH are the same as for Cu_3, Cu_4 and Cu_5. The free energy changes for odd and even ($H^+ + e^-$) pair transfer steps on Cu_6 exhibit similar exergonicity/endergonicity behaviour as for Cu_4. The RDS for CH_4 production is the formation of CHO* from CO*, with an endergonic free energy change of 0.709 eV, close to the value for Cu_4: 0.805 eV. The formation of CH_3OH proceeds through the same lowest energy route (Path V) found for the Cu_3, Cu_4 and Cu_5 clusters. The rate-limiting step is the formation of CHO* from CO* species as in the case of the CH_4 formation, however, the formation of the methanol is controlled by the more thermodynamically favoured methane formation (CH$_3$O* → CH_4 + *) step. On Cu_6, COOH* formation is mildly exergonic (-0.122 eV) and is comparable to the free energy change of -0.093 eV on Cu_4. The release of HCOOH in the second proton-electron transfer is the RDS which is mildly endergonic (0.032 eV) on Cu_6 and has a comparable RDS free energy change of 0.003 eV on Cu_4 cluster surface. However, the formation of HCOOH should compete with the formation of CO* from COOH* which is the thermodynamically highly favoured reaction step, with a

larger exergonic free energy release of -0.601 eV. The further reduction of adsorbed CO* to CHO* is thermodynamically slightly disfavoured with respect to the liberation of CO. The CO* desorption step and the CO* → CHO* step require free energies of 0.642 eV and 0.709 eV, respectively on Cu_6 which are comparable RDS free energy changes on Cu_4 (0.709 eV and 0.805 eV) for the same steps. The two-electron reduction pathways on Cu_6 also show a strong resemblance to those on Cu_4, analogous to the close resemblance of the reaction pathways on Cu_5 and Cu_3 clusters. As the formation of the higher reduction products is dependent on the feasibility of the adsorbed CO* species to form CHO*, we expect that production of methane and methanol is adversely affected by the more favourable CO release step on Cu_4 and Cu_6. In contrast, the formation of CHO* preferred over release of CO on Cu_3 and Cu_5.
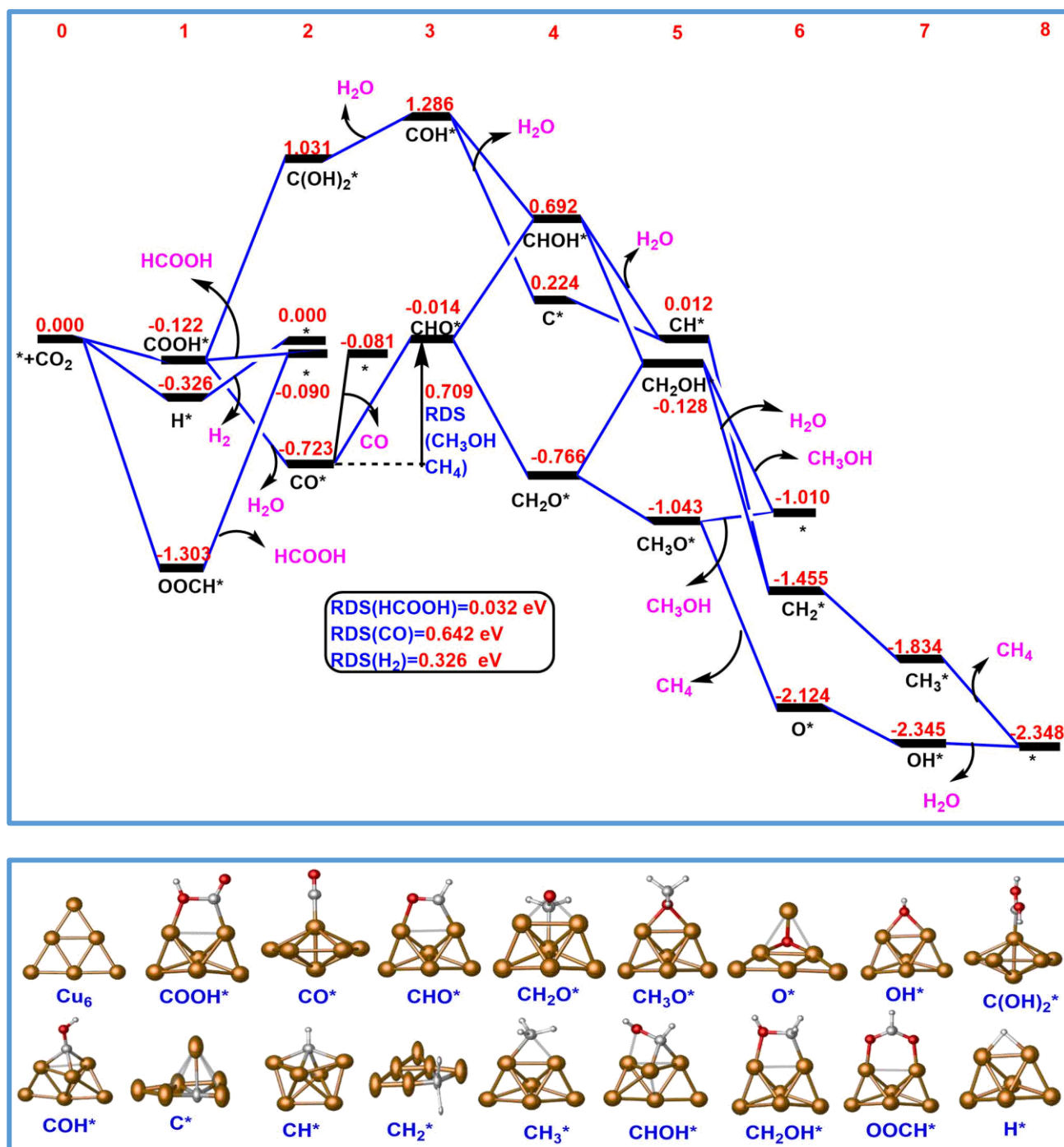

Figure 7: Free energy changes (ΔG; solvent-corrected, eV) calculated for the electrochemical pathways for the reduction of CO_2 on the Cu_6 cluster, employing the CHE model. The lowest energy geometries for the various adsorbed species are shown in the lower panel.
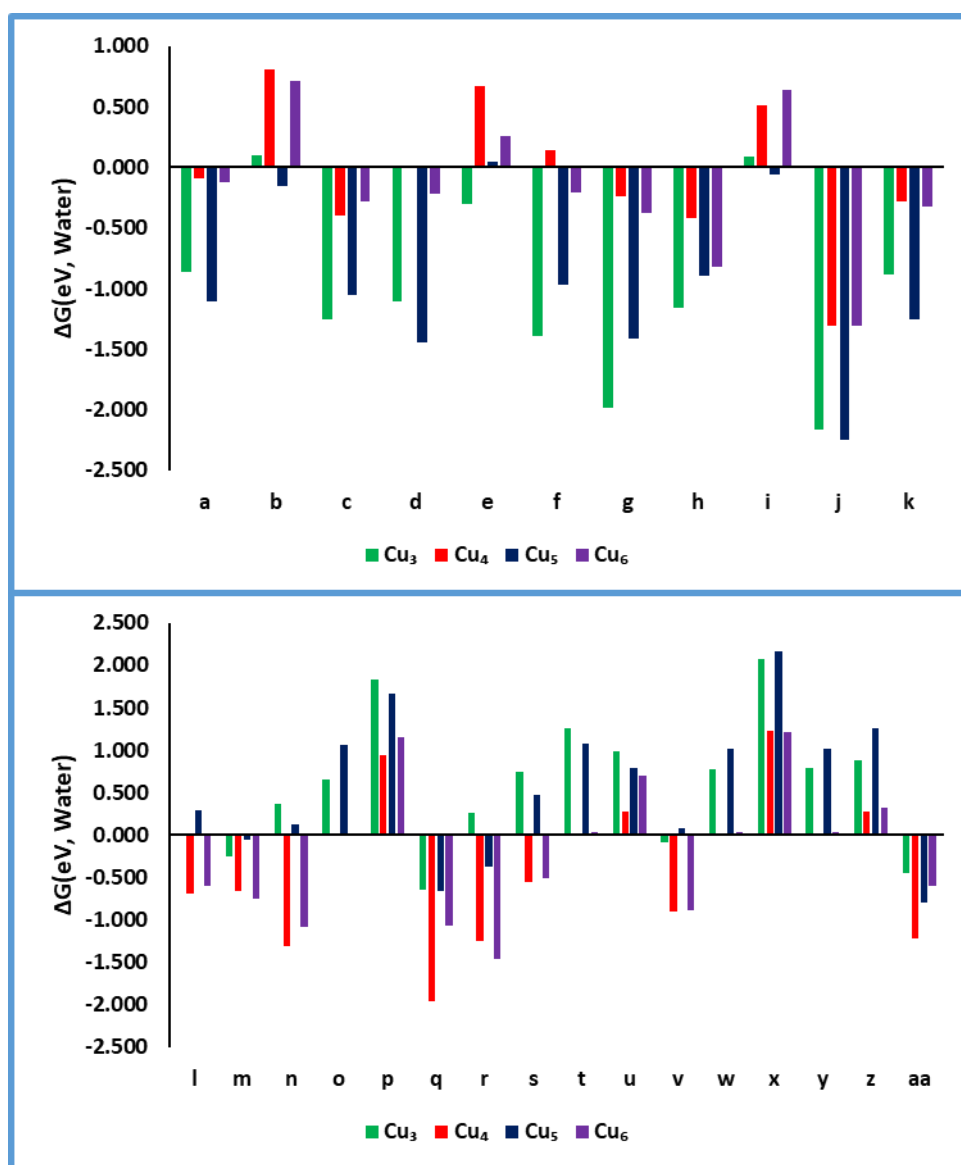
20

Figure 8: Free energy changes for different electrochemical steps that involve an odd (top) or an even number (bottom) of $(H^+ + e^-)$ pair transfers on the Cu_3, Cu_4, Cu_5 and Cu_6 clusters. See Table 2 for a description of each step and the spin states of the various cluster-adsorbate intermediates on the clusters.

As noted above, the extent to which a reaction step is uphill (endergonic) or downhill (exergonic) on a cluster is determined by the spin state of the intermediate cluster-adsorbate complex. A close inspection of Figure 8 reveals that the exergonicity and endergonicity of the steps shows a striking resemblance between Cu_3 and Cu_5 and between Cu_4 and Cu_6. In order to make this clearer, we have plotted the free energy change of each step for clusters possessing an even number of electrons (Cu_4 and Cu_6) with respect to clusters with an odd number of electrons (Cu_3 and Cu_5) in Figure 9. In general, those electrochemical steps (a-k) that involve an odd total number of $(H^+ + e^-)$ pair transfers, leading to the formation of doublet intermediates on Cu_4 and Cu_6 (Table 2) are endergonic ($\Delta G > 0$), whereas those steps (l-aa) that involve an even total number of $(H^+ + e^-)$ pair transfers, leading to the formation of singlet intermediates on Cu_4 and Cu_6 are exergonic ($\Delta G < 0$). Although, we have found an exception for step aa (COH* $\rightarrow$ CHOH*), the discrepancy can be attributed to the high free energy of CHOH* on Cu_6 compared to Cu_5, possibly due to rearrangement of the cluster core and/or due to the differences in the solvation effects, does not affect the overall trend in the exergonicity/endergonicity. Overall, however, the results for Cu_6 are in agreement with the conclusion that electrochemical proton-electron transfer steps going from doublet to singlet intermediates, are thermodynamically favourable. Conversely, proton-electron transfer steps going from singlet to doublet

intermediates, are thermodynamically unfavourable. It is also evident from our study that the energetic cost for the geometry rearrangement and solvation effects will also be reflected in the free energy changes for the various electrochemical steps and can affect the exergonicity/endergonicity of the electrochemical step.
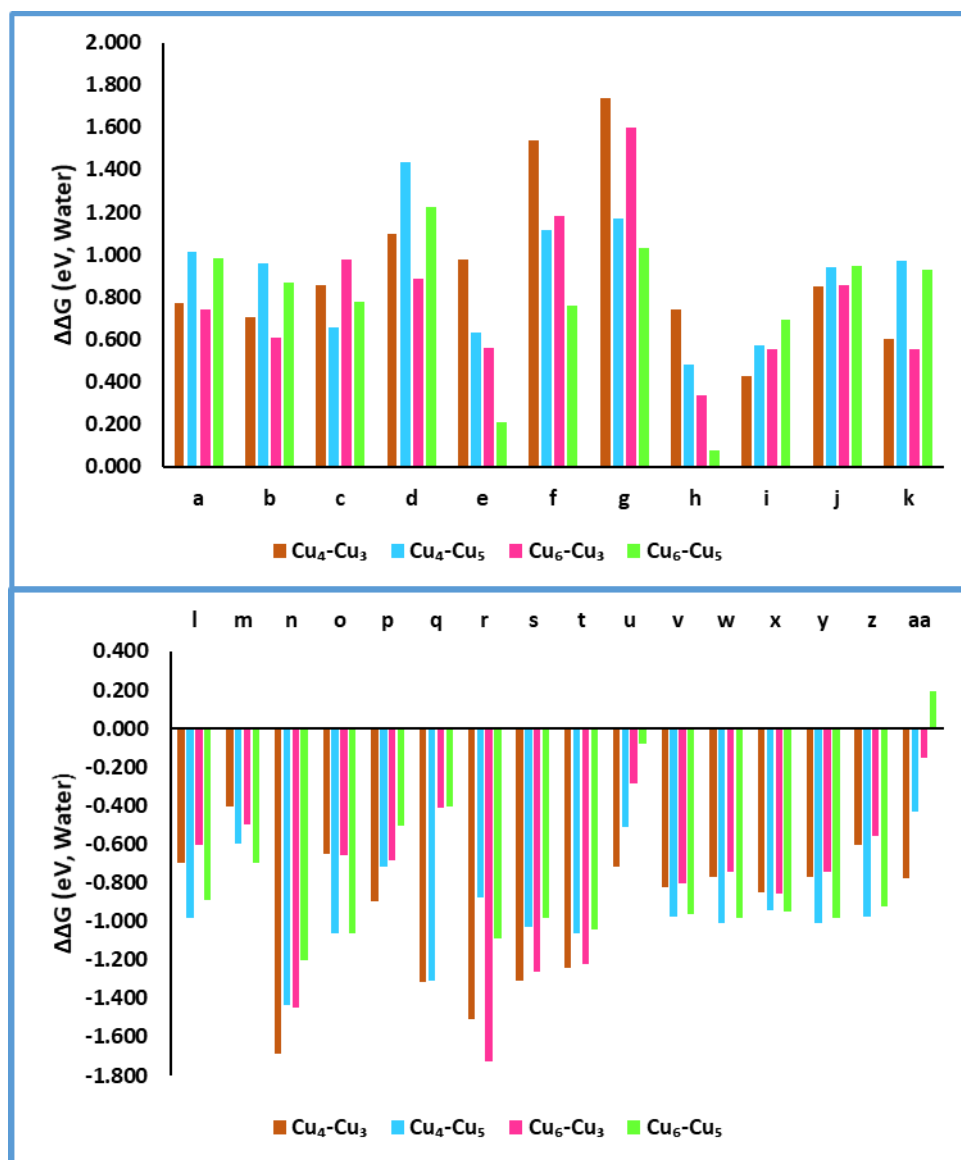
Figure 9: Ender/exergonicity for the various electrochemical steps that involve odd (top) or even total number (bottom) of $(H^+ + e^-)$ pair transfers on the Cu_4 and Cu_6 clusters relative to the ender/exergonicity on the Cu_3 and Cu_5 clusters.

(iv)   Correlation of exergonicity/endergonicity of CO2RR steps with HOMO-LUMO gaps for Cu_3-Cu_6 clusters

We have found a general relationship between the exergonicity and endergonicity of the various electrochemical steps and the HOMO-LUMO gap (Δ_{HL}) of the cluster-adsorbate intermediate species. The intermediates COOH*, CHO*, CH$_3$O*, OH*, COH*, CH*, CH$_3$*, CH$_2$OH*, OOCH* and H*, which have singlet ground spin states on the Cu_3 and Cu_5 clusters, have larger Δ_{HL} values in the range 0.23-0.28 eV. The same species adsorbed on Cu_4 and Cu_6 (which have doublet spin states) show relatively smaller HOMO-LUMO gaps, in the range 0.16-0.19 eV. The transfer of a proton-electron pair to these intermediates adsorbed on Cu_3 and Cu_5 are relatively difficult due to the large HOMO-LUMO gap and it is relatively easier to reduce adsorbates on Cu_4 and Cu_6, which have smaller Δ_{HL}. Hence, proton-electron pair transfer to these species on Cu_3 and Cu_5 clusters are in general more highly endergonic or have smaller exergonic free energy changes compared to

those on the Cu_4 and Cu_6 clusters. Although, there are some exceptions due to the energetic cost of cluster geometrical rearrangements, the trend in the endergonicity and exergonicity of the electrochemical steps that involve these species on Cu_3/Cu_5 or Cu_4/Cu_6 clusters support this argument.

Table 3: HOMO-LUMO gaps (Δ_{HL} / eV; solvent-corrected) of Cu clusters and the spin states for various adsorbed species.

	Cu_3	Cu_5	Cu_4	Cu_6
	Doublet Spin		Singlet Spin	
*	0.166	0.162	0.206	0.243
CO*	0.178	0.160	0.219	0.211
CH_2O*	0.223	0.218	0.217	0.222
O*	0.185	0.180	0.247	0.240
$C(OH)_2$*	0.206	0.220	0.226	0.210
C*	0.234	0.174	0.243	0.217
CH_2*	0.178	0.194	0.244	0.233
CHOH*	0.218	0.221	0.215	0.220
	Singlet Spin		Doublet Spin	
COOH*	0.262	0.252	0.172	0.156
CHO*	0.256	0.251	0.171	0.155
CH_3O*	0.282	0.243	0.174	0.156
OH*	0.250	0.243	0.176	0.157
COH*	0.229	0.227	0.191	0.193
CH*	0.257	0.227	0.158	0.163
CH_3*	0.268	0.243	0.171	0.157
CH_2OH*	0.250	0.249	0.172	0.156
OOCH*	0.275	0.249	0.172	0.156
H*	0.238	0.246	0.170	0.157

The doublet intermediates CO*, CH_2O*, O*, $C(OH)_2$*, C*, CH_2* and CHOH* on Cu_3 and Cu_5 have HOMO-LUMO gaps in the range 0.16-0.23 eV, whilst, Δ_{HL} lies in the range 0.21-0.25 eV on Cu_4 and Cu_6 (where these intermediates are singlets). While there is more overlap between the HOMO-LUMO gaps for the singlet and doublet states in these cases than for those mentioned above, again there is a correlation between higher Δ_{HL} values and more positive ΔG values for these reduction steps (with lower Δ_{HL} correlating with more negative ΔG). There are some exceptions, such as CH_2O* and CHOH*, which have similar HOMO-LUMO gaps for all four clusters. The electrochemical steps CH_2O* $\rightarrow$ CH_3O* and CHOH* $\rightarrow$ CH_2OH* are exergonic on all four clusters, though the exergonicity of the CH_2O* $\rightarrow$ CH_3O* step is significantly higher on Cu_3 and Cu_5 compared to Cu_4 and Cu_6, so it still follows the general trend. However, the exergonicity for the CHOH*$\rightarrow$$CH_2OH$* step on different Cu cluster surfaces do not follow this general trend. Despite having similar HOMO-LUMO gaps for the CHOH* species on different Cu clusters (Cu_3 0.218 eV; Cu_4 0.221 eV; Cu_5 0.215 eV; Cu_6 0.220 eV), we do not see similar exergonicities for the CHOH* $\rightarrow$ CH_2OH* step. For instance, CHOH* $\rightarrow$ CH_2OH* step is accompanied with an exergonic free energy changes of -1.156 eV, -0.416 eV, -0.898 eV and -0.820 eV, respectively on Cu_3, Cu_4, Cu_5 and Cu_6 cluster surfaces. The C* adsorbate on Cu_3, which is a doublet species, has a relatively large HOMO-LUMO gap of 0.234 eV, similar to the gaps for the singlet C* species on Cu_4 (0.243 eV) and Cu_6 (0.217 eV). However, the electrochemical step C* $\rightarrow$ CH* on Cu_3 has a large exergonic free energy change (-1.396 eV), similar to the Cu_5 cluster (-0.973 eV), where there is a smaller Δ_{HL} gap (0.174 eV). These discrepancies can be attributed to the high free energy state of the adsorbates, primarily due to the energetic cost of the cluster core rearrangement and/or due to solvation effects. These results emphasise that, in addition to the HOMO-LUMO gap of the adsorbed species, other factors, such as the relative stability of the intermediate species as well as the free energy cost of the geometric rearrangement of the cluster

core on ligand binding and solvation effects, contribute to the exergonicity or endergonicity of specific reaction steps.

To summarise our findings: electrochemical proton-electron transfer to doublet species, which generally have smaller HOMO-LUMO gaps, are thermodynamically more favourable, usually with exergonic free energy changes. In contrast, $(H^+ + e^-)$ pair transfers to singlet species, which generally have larger HOMO-LUMO gaps, are thermodynamically less favourable, usually with endergonic free energy changes. We, therefore, conclude that the spin state of the cluster-adsorbate intermediates is the primary factor that decides the degree of exergonicity or endergonicity of the various electrochemical steps on subnano clusters. In addition to this factor, the energetic cost for any geometrical rearrangement of the cluster core and solvation effects will also contribute to the overall endergonicity and exergonicity of each electrochemical step.

(v)   Limiting potentials for CO2RR on Cu_3-Cu_6 clusters

The limiting potentials (U_L), i.e. the potentials which must be applied to make the most endergonic step become exergonic, for the lowest energy pathways for the formation of CH_4, CH_3OH, HCOOH, CO and H_2 on Cu_3-Cu_6 can be easily determined from Table 4, using the relationship $\Delta G = -U_L/e$. The limiting potentials show the following orders: **Cu_3:** CH_4 < HCOOH < CO < H_2 < CH_3OH; **Cu_4:** HCOOH < H_2 < CO < CH_3OH, CH_4; **Cu_5:** CO < HCOOH < CH_4 < CH_3OH < H_2; **Cu_6:** HCOOH < H_2 < CO < CH_3OH, CH_4.

Table 4: The RDS and overall free energies (eV; solvent-corrected) for the electrochemical formation of CH_4, CH_3OH, HCOOH, CO and H_2 on the clusters Cu_3-Cu_6.

	Cu_3		Cu_4	
	RDS Step	**ΔG**	**RDS Step**	**ΔG**
CH_4	$OH^* + (H^+ + e^-) \rightarrow H_2O + *$	**0.655**	$CO^* + (H^+ + e^-) \rightarrow CHO^*$	**0.805**
CH_3OH	$CH_3O^* + (H^+ + e^-) \rightarrow * + CH_3OH$	**1.256**	$CO^* + (H^+ + e^-) \rightarrow CHO^*$	**0.805**
HCOOH	$COOH^* + (H^+ + e^-) \rightarrow HCOOH + *$	**0.774**	$COOH^* + (H^+ + e^-) \rightarrow HCOOH + *$	**0.003**
CO	$CO^* \rightarrow * + CO$ (non-electrochemical)	**0.784**	$CO^* \rightarrow * + CO$ (non-electrochemical)	**0.709**
H_2	$H^* + (H^+ + e^-) \rightarrow H_2 + *$	**0.881**	$H^* + (H^+ + e^-) \rightarrow H_2 + *$	**0.278**
	Cu_5		Cu_6	
	RDS Step	**ΔG**	**RDS Step**	**ΔG**
CH_4	$OH^* + (H^+ + e^-) \rightarrow H_2O + *$	**1.062**	$CO^* + (H^+ + e^-) \rightarrow CHO^*$	**0.709**
CH_3OH	$CH_3O^* + (H^+ + e^-) \rightarrow * + CH_3OH$	**1.075**	$CO^* + (H^+ + e^-) \rightarrow CHO^*$	**0.709**
HCOOH	$COOH^* + (H^+ + e^-) \rightarrow HCOOH + *$	**1.015**	$COOH^* + (H^+ + e^-) \rightarrow HCOOH + *$	**0.032**
CO	$CO^* \rightarrow * + CO$ (non-electrochemical)	**0.737**	$CO^* \rightarrow * + CO$ (non-electrochemical)	**0.642**
H_2	$H^* + (H^+ + e^-) \rightarrow H_2 + *$	**1.251**	$H^* + (H^+ + e^-) \rightarrow H_2 + *$	**0.326**

A negative potential of -0.655 V should be applied to make the limiting free energy step, i.e. the removal of the adsorbed OH* from the surface, exergonic on Cu_3. The opening of the CH_4 pathway happens first, at -0.655 V, followed by the HCOOH and CO pathways at -0.774 V and -0.783 V, respectively. It should be noted that methane selectivity is much higher on the Cu_3 cluster as the methanol only forms at a much higher applied potential (-1.256 V). Most interestingly, H_2 evolution, which is one of the unwanted side reactions that should be suppressed in the CO2RR, only starts at a higher negative potential (-0.881 V), which indicates that HER does not compete with the other pathways except for CH_3OH formation in the aqueous environment. On Cu_4, the opening of the HCOOH pathway occurs first, at almost zero overpotential, followed by the H_2 and CO pathways at -0.278 V and -0.709 V, respectively. The production of CH_4 and CH_3OH will be dominant only after attaining the higher limiting potential of 0.805 V. Though the limiting step is same for both CH_4 and CH_3OH, as discussed above, the formation of CH_4 is thermodynamically more favourable compared to CH_3OH. The requirement of a high limiting potential for hydrogen evolution on Cu_3 makes it a better catalyst than Cu_4 as the competing HER is more hindered on Cu_3 compared to Cu_4. Moreover, the opening of the CH_4 pathway begins at relatively low applied voltages on Cu_3 compared to Cu_4. A free energy profile at the applied voltage for Cu_3 and Cu_4 is shown in Figure 10. Similar graphs can be constructed for

other reactions pathways at the applied potential by shifting the free energy of each electrochemical step by eU_L.

Although the limiting steps are identical for Cu_5 and Cu_3 clusters, the opening of HCOOH and CH_4 pathways require much higher potentials on Cu_5. The CO pathway is the first one to open at -0.737 V followed by HCOOH at -1.015 V, CH_4 at -1.062, CH_3OH at -1.075 V and finally H_2 at -1.251 V. As the H_2 pathway is the last to open on the Cu_5 cluster, it can be predicted that HER does not compete with the other pathways. Yet, it should be remembered that the required potentials are much larger for the formation of CH_4, CH_3OH and HCOOH on the Cu_5 cluster. The limiting steps are identical with similar range of limiting potential values on Cu_4 and Cu_6 clusters. Similarly on Cu_4, the HCOOH pathway will open first, followed by the H_2 and CO pathways on Cu_6. The limiting step (CO* → CHO*) for the formation of CH_4 and CH_3OH on the Cu_6 cluster requires an applied potential of -0.709 V which is comparable to the limiting potential of -0.805 V on Cu_4. We have found that the H_2 pathway will open at relatively lower potentials on the Cu_4 and Cu_6 clusters compared to those on the Cu_3 and Cu_5 clusters. As the limiting potentials for the H_2 pathway opens at much higher potentials, the HER side reaction will be suppressed on the Cu_3 and Cu_5 clusters.
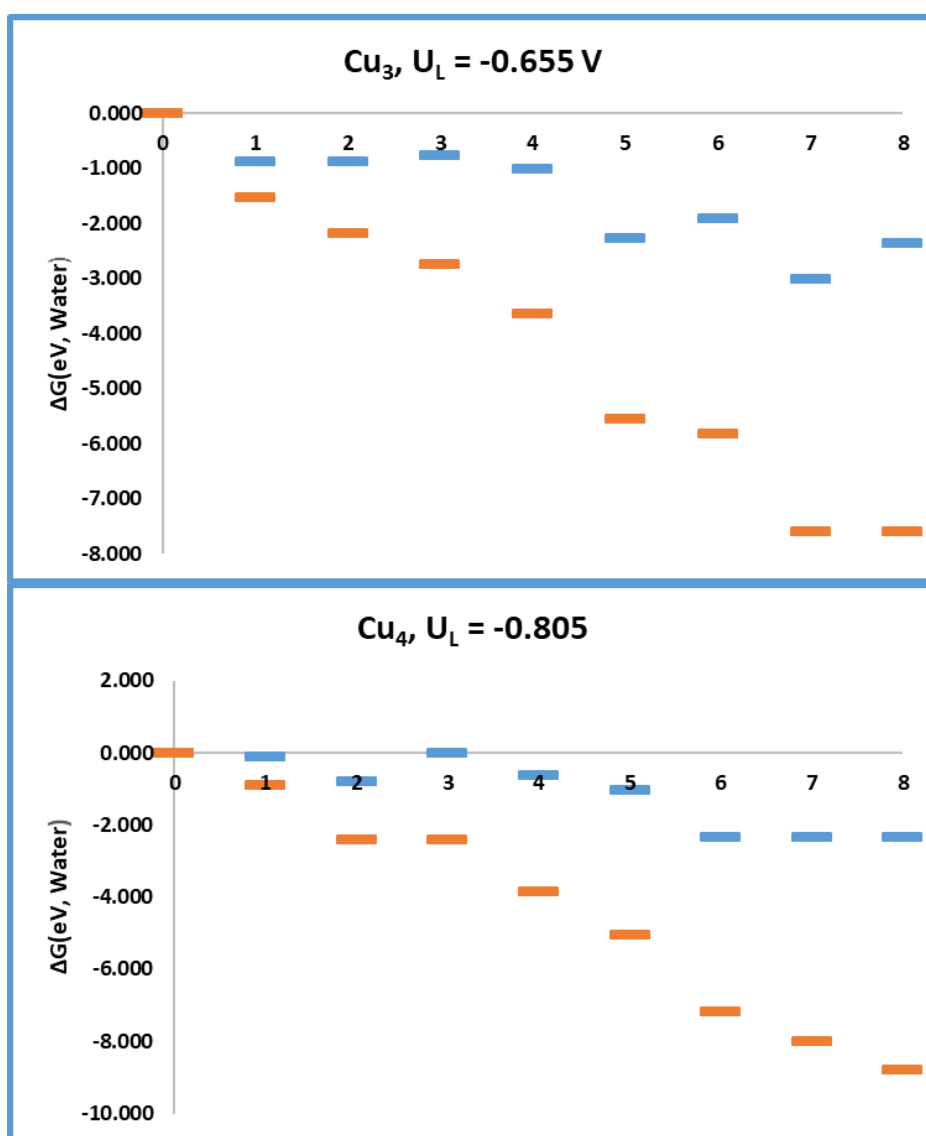

Figure 10: Free energy changes for the reaction pathways for the formation of CH_4 on Cu_3 and Cu_4 clusters at zero applied voltage (U=0, Blue) and at the limiting applied potential (U_L, Orange). The numbers 1 to 8 corresponds to each ($H^+ + e^-$) transfer steps for the lowest energy route (Path I) (* + CO_2 → COOH* → CO* + H_2O → CHO* → CH_2O* → CH_3O* → CH_4 + O* → OH* → *+ H_2O).

Comparison of CO₂RR on copper clusters and copper surfaces

Nørskov *et al.* have reported that the key potential limiting step on the Cu(211) surface is the proton-electron pair transfer to the adsorbed species CO* to form CHO* and that the efficiency of the CO2RR can be enhanced if the stability of the CHO* species is higher than CO*, which reduces the overpotential.[27] We have found from our studies that the CO2RR on the even-electron Cu_4 and Cu_6 clusters resembles the copper surface more closely than the odd-electron Cu_3 and Cu_5 clusters do. The rate-limiting step for the production of CH_4 on the Cu_4 and Cu_6 clusters is the same (CO* → CHO*) as for the copper surface. The limiting potentials for this key step on Cu_4 and Cu_6 clusters are -0.805 V and -0.709 V, respectively, which is comparable to the value (-0.74 V) reported for the Cu(211) surface by Nørskov.[27] The HER is the first electrochemical pathway to open on the Cu(211) surface, at an applied voltage of -0.03 V (with no solvation correction) [27] which is close to the gas-phase limiting potential values we have calculated on the Cu_4 (-0.050 V) and Cu_6 (-0.067 V) clusters (See Supplementary information). As for the Cu(211) surface, at lower potentials the two-electron reduction products H_2, HCOOH, CO are dominant on Cu_4 and Cu_6 clusters.

Conclusions

We have performed a detailed investigation of the electrocatalytic activity of size-selected Cu_n clusters (n=3-6) for CO_2 reduction, employing the Computational Hydrogen Electrode model. We have found a striking similarity between CO2RR activity of the odd-electron Cu_3 and Cu_5 clusters and between the even-electron Cu_4 and Cu_6 clusters. The reaction proceeds through the following steps: * + CO_2 → COOH* → CO* + H_2O → CHO* → CH_2O* → CH_3O → O* + CH_4 → OH* → * + H_2O on all the Cu clusters for the production of the eight-electron reduction product methane, as has previously been found from computations on the Cu(211) surface. On the Cu_4 and Cu_6 clusters, the RDS is the proton-electron transfer to the adsorbed CO* species to form CHO*, whilst the removal of the adsorbed OH* from the cluster surface (OH* → * + H_2O) is the RDS on the Cu_3 and Cu_5 clusters. Most importantly, we have identified a general trend in the exergonicity and endergonicity of each step with the spin-state of the nanocluster. In general, those electrochemical steps that involve an odd total number of (H^+ + e^-) pair transfers, leading to the formation of doublet adsorbed species on Cu_4 and Cu_6 are more endergonic processes relative to the same steps on the Cu_3 and Cu_5 clusters, i.e. $\Delta\Delta G = \Delta G(Cu_{4,6}) - \Delta G(Cu_{3,5}) > 0$. Conversely, those steps that involve an even total number of proton-electron pair transfers, leading to the formation of singlet adsorbed species on Cu_4 and Cu_6, are more exergonic processes ($\Delta\Delta G < 0$) relative to the same steps on Cu_3 and Cu_5. We have also found that the competing hydrogen evolution reaction (HER) is more hindered on Cu_3 and Cu_5 compared to the Cu_4 and Cu_6 clusters. We have found that CH_4 vs. CH_3OH selectivity depends on the competing steps CH_3O* → O* + CH_4 and CH_3O* → * + CH_3OH and our computations reveal greater selectivity for CH_4 on these sub-nanometre clusters, as in the case of copper surfaces.

We have also investigated the relationship between the free energies of the various electrochemical steps and the HOMO-LUMO gaps of the cluster-adsorbate complex intermediates. The general finding is that cluster-adsorbate intermediates with singlet spin states (even total number of electrons = closed shell) typically have higher HOMO-LUMO gaps than doublet spin states (odd number of electrons = open shell). The larger HOMO-LUMO gaps are typically associated with higher stability (lower free energy of the intermediates). Hence, singlet→doublet electron transfer steps tend to have $\Delta G > 0$ (or are more endergonic/less exergonic) and doublet→singlet steps tend to have $\Delta G < 0$ (or are more exergonic/less endergonic). Finally, we note that, in addition to these effects based on the relative stabilities of singlet and doublet intermediates, the energetic cost of any geometrical rearrangements of the cluster core and solvation effects will also affect the magnitude of the exergonicity or endergonicity of each electrochemical step.

Acknowledgments

References

(1)   Dlugokencky, E.; Tans, P. (NOAA/ESRL). Trends in Atmospheric Carbon Dioxide: Recent Global CO_2.

(2)   NOAA National Centers for Environmental Information, State of the Climate: Global Analysis for Annual 2017, Published Online January 2018, Retrieved on Septmber 24, 2018 from *Http://Www.Ncdc.Noaa.Gov/Sotc/Global/201713.*

(3)   Eppinger, J.; Huang, K.-W. Formic Acid as a Hydrogen Energy Carrier. *ACS Energy Lett.* **2017**, *2* (1), 188–195.

(4)   Olah, G. A. Beyond Oil and Gas: The Methanol Economy. *Angew. Chem. Int. Ed. Engl.* **2005**, *44*, 2636.

(5)   Kondratenko, E. V.; Mul, G.; Baltrusaitis, J.; Larrazábal, G. O.; Pérez-Ramírez, J. Status and Perspectives of CO_2 Conversion into Fuels and Chemicals by Catalytic, Photocatalytic and Electrocatalytic Processes. *Energy Environ. Sci.* **2013**, *6*, 3112.

(6)   Saeidi, S.; Amin, N. A. S.; Rahimpour, M. R. Hydrogenation of CO_2 to Value-Added Products—A Review and Potential Future Developments. *J. CO2 Util.* **2014**, *5*, 66–81.

(7)   Jadhav, S. G.; Vaidya, P. D.; Bhanage, B. M.; Joshi, J. B. Catalytic Carbon Dioxide Hydrogenation to Methanol: A Review of Recent Studies. *Chem. Eng. Res. Des.* **2014**, *92*, 2557–2567.

(8)   Zhu, D. D.; Liu, J. X. L.; Qiao, S. Z.; Zhang, H.; Liu, G.; Shi, L.; Ye, J.; Zhang, W.; Hu, Y.; Ma, L.; et al. Progress and Perspective of Electrocatalytic CO_2 Reduction for Renewable Carbonaceous Fuels and Chemicals. *J. Am. Chem. Soc.* **2018**, *5* (1), 3423–3452.

(9)   Zhu, D. D.; Liu, J. L.; Qiao, S. Z. Recent Advances in Inorganic Heterogeneous Electrocatalysts for Reduction of Carbon Dioxide. *Adv. Mater.* **2016**, *28* (18), 3423–3452.

(10)   Zhang, L.; Zhao, Z.-J.; Gong, J. Nanostructured Materials for Heterogeneous Electrocatalytic CO_2 Reduction and Their Related Reaction Mechanisms. *Angew. Chemie Int. Ed.* **2017**, 11326–11353.

(11)   Qiao, J.; Liu, Y.; Hong, F.; Zhang, J. *A Review of Catalysts for the Electroreduction of Carbon Dioxide to Produce Low-Carbon Fuels.*; 2014; Vol. 43.

(12)   Li, F.; MacFarlane, D.; Zhang, J. Recent Advances in Nanoengineering of Electrocatalysts for CO_2 Reduction. *Nanoscale* **2018**, 6235–6260.

(13)   Li, Y.; Chan, S. H.; Sun, Q. Heterogeneous Catalytic Conversion of CO_2: A Comprehensive Theoretical Review. *Nanoscale* **2015**, *7* (19), 8663–8683.

(14)   Kumar, B.; Brian, J. P.; Atla, V.; Kumari, S.; Bertram, K. A.; White, R. T.; Spurgeon, J. M. New Trends in the Development of Heterogeneous Catalysts for Electrochemical CO_2 Reduction. *Catal. Today* **2016**, *270*, 19.

(15)   Duan, X.; Xu, J.; Wei, Z.; Ma, J.; Guo, S.; Wang, S.; Liu, H.; Dou, S. Metal-Free Carbon Materials for CO_2 Electrochemical Reduction. *Adv. Mater.* **2017**, *1701784*, 1701784.

(16)   Raciti, D.; Wang, C. Recent Advances in CO_2 Reduction Electrocatalysis on Copper. *ACS Energy Lett.* **2018**, *3*, 1545.

(17)   Li, W. Electrocatalytic Reduction of CO_2 to Small Organic Molecule Fuels on Metal Catalysts. In *Electrocatalytic Reduction of CO_2 to Small Organic Molecule Fuels on Metal Catalysts, In Advances in CO_2 Conversion and Utilization*; ACS Symposium Series, Vol 1056, 2010; Vol. 1056, pp 55–76.

(18)   Hori, Y. Electrochemical CO_2 Reudction on Metal Electrodes. In *Electrochemical CO_2 Reudction on Metal Electrodes In Modern Aspects of Electrochemistry, Vol. 42*; Springer New York, 2008; p 89.

(19)   Gattrell, M.; Gupta, N.; Co, A. A Review of the Aqueous Electrochemical Reduction of CO_2 to Hydrocarbons at Copper. *Journal of Electroanalytical Chemistry*. 2006, pp 1–19.

(20)   Cook, R. L. Evidence for Formaldehyde, Formic Acid, and Acetaldehyde as Possible Intermediates during Electrochemical Carbon Dioxide Reduction at Copper. *J. Electrochem. Soc.* **1989**, *136* (7), 1982.

(21)   DeWulf, D. W. Electrochemical and Surface Studies of Carbon Dioxide Reduction to Methane and Ethylene at Copper Electrodes in Aqueous Solutions. *J. Electrochem. Soc.* **1989**, *136* (6), 1686.

(22)   Hori, Y.; Murata, A.; Takahashi, R. Formation of Hydrocarbons in the Electrochemical Reduction of Carbon Dioxide at a Copper Electrode in Aqueous Solution. **1989**, *85* (8), 2309–2326.

(23)   Hori, Y.; Wakebe, H.; Tsukamoto, T.; Koga, O. Electrocatalytic Process of CO Selectivity in Electrochemical Reduction of CO_2 at Metal Electrodes in Aqueous Media. *Electrochim. Acta* **1994**, *39* (11–12), 1833–1839.

(24)   Kim, J. J.; Summers, D. P.; Frese, K. W. Reduction of CO_2 and CO to Methane on Cu Foil Electrodes. *J. Electroanal. Chem.* **1988**, *245* (1–2), 223–244.

(25)   Whipple, D. T.; Kenis, P. J. a. Prospects of CO_2 Utilization via Direct Heterogeneous Electrochemical Reduction. *J. Phys. Chem. Lett.* **2010**, *1* (24), 3451–3458.

(26)   Kortlever, R.; Shen, J.; Schouten, K. J. P.; Calle-Vallejo, F.; Koper, M. T. M. Catalysts and Reaction Pathways for the Electrochemical Reduction of Carbon Dioxide. *J. Phys. Chem. Lett.* **2015**, *6* (20), 4073.

(27)   Peterson, A. A.; Abild-Pedersen, F.; Studt, F.; Rossmeisl, J.; Nørskov, J. K. How Copper Catalyzes the Electroreduction of Carbon Dioxide into Hydrocarbon Fuels. *Energy Environ. Sci.* **2010**, *3* (9), 1311–1315.

(28)   Nie, X.; Esopi, M. R.; Janik, M. J.; Asthagiri, A. Selectivity of CO_2 Reduction on Copper Electrodes: The Role of the Kinetics of Elementary Steps. *Angew. Chemie - Int. Ed.* **2013**, *52* (9), 2459–2462.

(29)   Nie, X.; Luo, W.; Janik, M. J.; Asthagiri, A. Reaction Mechanisms of CO_2 Electrochemical Reduction on Cu(111) Determined with Density Functional Theory. *J. Catal.* **2014**, *312*, 108–122.

(30)   Kuhl, K. P.; Cave, E. R.; Abram, D. N.; Jaramillo, T. F. New Insights into the Electrochemical Reduction of Carbon Dioxide on Metallic Copper Surfaces. *Energy Environ. Sci.* **2012**, *5* (5), 7050–7059.

(31)   Garza, A. J.; Bell, A. T.; Head-Gordon, M. Mechanism of CO_2 Reduction at Copper Surfaces: Pathways to C_2 Products. *ACS Catal.* **2018**, *8* (2), 1490–1499.

(32)   Schouten, K. J. P.; Kwon, Y.; van der Ham, C. J. M.; Qin, Z.; Koper, M. T. M. A New Mechanism for the Selectivity to C1 and C2 Species in the Electrochemical Reduction of Carbon Dioxide on Copper Electrodes. *Chem. Sci.* **2011**, *2* (10), 1902–1909.

(33)   Schouten, K. J. P.; Qin, Z.; Gallent, E. P.; Koper, M. T. M. Two Pathways for the Formation of Ethylene in CO Reduction on Single-Crystal Copper Electrodes. *J. Am. Chem. Soc.* **2012**, *134* (24), 9864–9867.

(34)   Calle-Vallejo, F.; Koper, M. T. M. Theoretical Considerations on the Electroreduction of CO to C_2 Species on Cu(100) Electrodes. *Angew. Chemie - Int. Ed.* **2013**, *52* (28), 7282–7285.

(35) Montoya, J. H.; Peterson, A. A.; Nørskov, J. K. Insights into C-C Coupling in CO_2 Electroreduction on Copper Electrodes. *ChemCatChem* **2013**, *5* (3), 737–742.

(36) Hussain, J.; Jonsson, H.; Skulason, E. Calculations of Product Selectivity in Electrochemical CO_2 Reduction. *ACS Catal.* **2018**.

(37) Liu, X.; Xiao, J.; Peng, H.; Hong, X.; Chan, K.; Nørskov, J. K. Understanding Trends in Electrochemical Carbon Dioxide Reduction Rates. *Nat. Commun.* **2017**, *8*, 15438.

(38) Chakraborty, I.; Pradeep, T. Atomically Precise Clusters of Noble Metals: Emerging Link between Atoms and Nanoparticles. *Chem. Rev.* **2017**, *117* (12), 8208–8271.

(39) Liu, L.; Corma, A. Metal Catalysts for Heterogeneous Catalysis: From Single Atoms to Nanoclusters and Nanoparticles. *Chem. Rev.* **2018**, *118* (10), 4981–5079.

(40) Dai, Y.; Wang, Y.; Liu, B.; Yang, Y. Metallic Nanocatalysis: An Accelerating Seamless Integration with Nanotechnology. *Small* **2015**, *11* (3), 268–289.

(41) Tyo, E. C.; Vajda, S. Catalysis by Clusters with Precise Numbers of Atoms. *Nat. Nanotechnol.* **2015**, *10* (7), 577–588.

(42) Liu, Y.; Li, Q.; Si, R.; Li, G. D.; Li, W.; Liu, D. P.; Wang, D.; Sun, L.; Zhang, Y.; Zou, X. Coupling Sub-Nanometric Copper Clusters with Quasi-Amorphous Cobalt Sulfide Yields Efficient and Robust Electrocatalysts for Water Splitting Reaction. *Adv. Mater.* **2017**, *29* (13), 1606200.

(43) Corma, A.; Concepción, P.; Boronat, M.; Sabater, M. J.; Navas, J.; Yacaman, M. J.; Larios, E.; Posadas, A.; López-Quintela, M. A.; Buceta, D.; et al. Exceptional Oxidation Activity with Size-Controlled Supported Gold Clusters of Low Atomicity. *Nat. Chem.* **2013**, *5* (9), 775–781.

(44) Lopez-Acevedo, O.; Kacprzak, K. A.; Akola, J.; Häkkinen, H. Quantum Size Effects in Ambient CO Oxidation Catalysed by Ligand-Protected Gold Clusters. *Nat. Chem.* **2010**, *2* (4), 329–334.

(45) Kaden, W. E.; Wu, T.; Kunkel, W. A.; Anderson, S. L. Electronic Structure Controls Reactivity of Size-Selected Pd Clusters Adsorbed on TiO_2 surfaces. *Science (80-.).* **2009**, *326* (5954), 826–829.

(46) Nesselberger, M.; Roefzaad, M.; Fayçal Hamou, R.; Ulrich Biedermann, P.; Schweinberger, F. F.; Kunz, S.; Schloegl, K.; Wiberg, G. K. H.; Ashton, S.; Heiz, U.; et al. The Effect of Particle Proximity on the Oxygen Reduction Rate of Size-Selected Platinum Clusters. *Nat. Mater.* **2013**, *12* (10), 919–924.

(47) Tian, S.; Fu, Q.; Chen, W.; Feng, Q.; Chen, Z.; Zhang, J.; Cheong, W.-C.; Yu, R.; Gu, L.; Dong, J.; et al. Carbon Nitride Supported Fe_2 Cluster Catalysts with Superior Performance for Alkene Epoxidation. *Nat. Commun.* **2018**, *9* (1), 2353.

(48) Vajda, S.; Pellin, M. J.; Greeley, J. P.; Marshall, C. L.; Curtiss, L. A.; Ballentine, G. A.; Elam, J. W.; Catillon-Mucherie, S.; Redfern, P. C.; Mehmood, F.; et al. Subnanometre Platinum Clusters as Highly Active and Selective Catalysts for the Oxidative Dehydrogenation of Propane. *Nat. Mater.* **2009**, *8* (3), 213–216.

(49) Mistry, H.; Reske, R.; Zeng, Z.; Zhao, Z.-J.; Greeley, J.; Strasser, P.; Cuenya, B. R. Exceptional Size-Dependent Activity Enhancement in the Electroreduction of CO_2 over Au Nanoparticles. *J. Am. Chem. Soc.* **2014**, *136* (47), 16473–16476.

(50) Kauffman, D. R.; Alfonso, D.; Matranga, C.; Ohodnicki, P.; Deng, X.; Siva, R. C.; Zeng, C.; Jin, R. Probing Active Site Chemistry with Differently Charged Au_{25}^{q} Nanoclusters (q = −1, 0, +1). *Chem. Sci.* **2014**, *5* (8), 3151.

(51) Kauffman, D. R.; Alfonso, D.; Matranga, C.; Qian, H.; Jin, R. Experimental and Computational Investigation of Au_{25} Clusters and CO_2: A Unique Interaction and Enhanced Electrocatalytic Activity. *J. Am. Chem. Soc.* **2012**, *134* (24), 10237–10243.

(52) Kim, C.; Jeon, H. S.; Eom, T.; Jee, M. S.; Kim, H.; Friend, C. M.; Min, B. K.; Hwang, Y. J. Achieving Selective and Efficient Electrocatalytic Activity for CO_2 Reduction Using Immobilized Silver Nanoparticles. *J. Am. Chem. Soc.* **2015**, *137* (43), 13844–13850.

(53) Salehi-Khojin, A.; Jhong, H. R. M.; Rosen, B. A.; Zhu, W.; Ma, S.; Kenis, P. J. A.; Masel, R. I. Nanoparticle Silver Catalysts That Show Enhanced Activity for Carbon Dioxide Electrolysis. *J. Phys. Chem. C* **2013**, *117* (4), 1627–1632.

(54) Gao, D.; Zhou, H.; Wang, J.; Miao, S.; Yang, F.; Wang, G.; Wang, J.; Bao, X. Size-Dependent Electrocatalytic Reduction of CO_2 over Pd Nanoparticles. *J. Am. Chem. Soc.* **2015**, *137* (13), 4288–4291.

(55) Zhang, Z.; Chi, M.; Veith, G. M.; Zhang, P.; Lutterman, D. A.; Rosenthal, J.; Overbury, S. H.; Dai, S.; Zhu, H. Rational Design of Bi Nanoparticles for Efficient Electrochemical CO_2 Reduction: The Elucidation of Size and Surface Condition Effects. *ACS Catal.* **2016**, *6* (9), 6255–6264.

(56) Zhao, C.; Dai, X.; Yao, T.; Chen, W.; Wang, X.; Wang, J.; Yang, J.; Wei, S.; Wu, Y.; Li, Y. Ionic Exchange of Metal-Organic Frameworks to Access Single Nickel Sites for Efficient Electroreduction of CO_2. *J. Am. Chem. Soc.* **2017**, *139* (24), 8078–8081.

(57) Zhang, S.; Kang, P.; Meyer, T. J. Nanostructured Tin Catalysts for Selective Electrochemical Reduction of Carbon Dioxide to Formate. *J. Am. Chem. Soc.* **2014**, *136* (5), 1734–1737.

(58) Tang, W.; Peterson, A. A.; Varela, A. S.; Jovanov, Z. P.; Bech, L.; Durand, W. J.; Dahl, S.; Nørskov, J. K.; Chorkendorff, I. The Importance of Surface Morphology in Controlling the Selectivity of Polycrystalline Copper for CO_2 Electroreduction. *Phys. Chem. Chem. Phys.* **2012**, *14* (1), 76–81.

(59) Reske, R.; Mistry, H.; Behafarid, F.; Roldan Cuenya, B.; Strasser, P. Particle Size Effects in the Catalytic Electroreduction of CO_2 on Cu Nanoparticles. *J. Am. Chem. Soc.* **2014**, *136* (19), 6978–6986.

(60) Passalacqua, R.; Parathoner, S.; Centi, G.; Halder, A.; Tyo, E. C.; Yang, B.; Seifert, S.; Vajda, S. Electrochemical Behaviour of Naked Sub-Nanometre Sized Copper Clusters and Effect of CO_2. *Catal. Sci. Technol.* **2016**, *6* (18), 6977–6985.

(61) Yang, X. F.; Wang, A.; Qiao, B.; Li, J.; Liu, J.; Zhang, T. Single-Atom Catalysts: A New Frontier in Heterogeneous Catalysis. *Acc. Chem. Res.* **2013**, *46* (8), 1740–1748.

(62) Zhang, H.; Liu, G.; Shi, L.; Ye, J. Single-Atom Catalysts: Emerging Multifunctional Materials in Heterogeneous Catalysis. *Adv. Energy Mater.* **2018**, *8* (1), 1701343.

(63) Wang, Y.; Chen, Z.; Han, P.; Du, Y.; Gu, Z.; Xu, X.; Zheng, G. Single-Atomic Cu with Multiple Oxygen Vacancies on Ceria for Electrocatalytic CO_2 Reduction to CH_4. *ACS Catal.* **2018**, *8* (8), 7113–7119.

(64) Jia, M.; Fan, Q.; Liu, S.; Qiu, J.; Sun, Z. Single-Atom Catalysis for Electrochemical CO_2 Reduction. *Curr. Opin. Green Sustain. Chem.* **2019**, *16*, 1–6.

(65) Back, S.; Lim, J.; Kim, N. Y.; Kim, Y. H.; Jung, Y. Single-Atom Catalysts for CO_2 electroreduction with Significant Activity and Selectivity Improvements. *Chem. Sci.* **2017**, *8* (2), 1090–1096.

(66) Duff, C. Ø. S. Le; Lawrence, M. J.; Rodriguez, P. Role of the Adsorbed Oxygen Species in the Selective Electrochemical Reduction of CO_2 to Alcohols and Carbonyls on Copper Electrodes. *Angew. Chemie*

2017, *129*, 13099–13104.

(67)   Liu, C.; Yang, B.; Tyo, E.; Seifert, S.; DeBartolo, J.; von Issendorff, B.; Zapol, P.; Vajda, S.; Curtiss, L. A. Carbon Dioxide Conversion to Methanol over Size-Selected Cu_4 Clusters at Low Pressures. *J. Am. Chem. Soc.* **2015**, *137* (27), 8676–8679.

(68)   Yang, B.; Liu, C.; Halder, A.; Tyo, E. C.; Martinson, A. B. F.; Seifert, S.; Zapol, P.; Curtiss, L. A.; Vajda, S. Copper Cluster Size Effect in Methanol Synthesis from CO_2. *J. Phys. Chem. C* **2017**, *121* (19), 10406–10412.

(69)   Rawat, K. S.; Mahata, A.; Pathak, B. Thermochemical and Electrochemical CO_2 Reduction on Octahedral Cu Nanocluster: Role of Solvent towards Product Selectivity. *J. Catal.* **2017**, *349*, 118–127.

(70)   Dong, H.; Li, Y.; Jiang, D. First-Principles Insight into Electrocatalytic Reduction of CO_2 to CH_4 on a Copper Nanoparticle. *J. Phys. Chem. C* **2018**, *122* (21), 11392–11398.

(71)   Liu, C.; He, H.; Zapol, P.; Curtiss, L. a. Computational Studies of Electrochemical CO_2 Reduction on Subnanometer Transition Metal Clusters. *Phys. Chem. Chem. Phys.* **2014**, *16* (48), 26584–26599.

(72)   Shanmugam, R.; Thamaraichelvan, A.; Ganesan, T. K.; Viswanathan, B. Computational Evaluation of Sub-Nanometer Cluster Activity of Singly Exposed Copper Atom with Various Coordinative Environment in Catalytic CO_2 transformation. *Appl. Surf. Sci.* **2017**, *396*, 444–454.

(73)   Nørskov, J. K.; Rossmeisl, J.; Logadottir, A.; Lindqvist, L.; Kitchin, J. R.; Bligaard, T.; Jónsson, H. Origin of the Overpotential for Oxygen Reduction at a Fuel-Cell Cathode. *J. Phys. Chem. B* **2004**, *108* (46), 17886.

(74)   Davis, J. B. A.; Shayeghi, A.; Horswell, S. L.; Johnston, R. L. The Birmingham Parallel Genetic Algorithm and Its Application to the Direct DFT Global Optimisation of Ir_N (N = 10–20) Clusters. *Nanoscale* **2015**, *7* (33), 14032–14038.

(75)   https://bitbucket.org/JBADavis/bpga/.

(76)   Deaven, D. M.; Ho, K. M. Molecular Geometry Optimization with a Genetic Algorithm. *Phys. Rev. Lett.* **1995**, *75* (2), 288–291.

(77)   Kresse, G.; Hafner, J. Ab Initio Molecular Dynamics for Liquid Metals. *Phys. Rev. B* **1993**, *47* (1), 558–561.

(78)   Kresse, G.; Hafner, J. Ab Initio Molecular-Dynamics Simulation of the Liquid-Metalamorphous-Semiconductor Transition in Germanium. *Phys. Rev. B* **1994**, *49* (20), 14251–14269.

(79)   Kresse, G.; Furthmüller, J. Efficient Iterative Schemes for Ab Initio Total-Energy Calculations Using a Plane-Wave Basis Set. *Phys. Rev. B - Condens. Matter Mater. Phys.* **1996**, *54* (16), 11169–11186.

(80)   Kresse, G.; Furthmüller, J. Efficiency of Ab-Initio Total Energy Calculations for Metals and Semiconductors Using a Plane-Wave Basis Set. *Comput. Mater. Sci.* **1996**, *6* (1), 15–50.

(81)   Joubert, D. From Ultrasoft Pseudopotentials to the Projector Augmented-Wave Method. *Phys. Rev. B - Condens. Matter Mater. Phys.* **1999**, *59* (3), 1758–1775.

(82)   Perdew, J. P.; Burke, K.; Ernzerhof, M. Generalized Gradient Approximation Made Simple. *Phys. Rev. Lett.* **1996**, *77* (18), 3865–3868.

(83)   Methfessel, M.; Paxton, A. T. High-Precision Sampling for Brillouin-Zone Integration in Metals. *Phys. Rev. B* **1989**, *40* (6), 3616–3621.

(84)   Frisch, M. J.; Trucks, G. W.; Schlegel, H. B.; Scuseria, G. E.; Robb, M. A.; Cheeseman, J. R.; Scalmani, G.; Barone, V.; Mennucci, B.; Petersson, G. A.; Nakatsuji, H.; Caricato, M.; Li, X.; Hratchian, H. P.; Izmaylov, A. F.; Bloino, J.; Zheng, G.; Sonnenb, D. J. Gaussian Program. *Gaussian 09, Revison E.01, Gaussian, Inc. Wallingford CT* **2009**.

(85)   Chai, J. Da; Head-Gordon, M. Long-Range Corrected Hybrid Density Functionals with Damped Atom-Atom Dispersion Corrections. *Phys. Chem. Chem. Phys.* **2008**, *10* (44), 6615–6620.

(86)   Weigend, F.; Ahlrichs, R. Balanced Basis Sets of Split Valence, Triple Zeta Valence and Quadruple Zeta Valence Quality for H to Rn: Design and Assessment of Accuracy. *Phys. Chem. Chem. Phys.* **2005**, *7* (18), 3297–3305.

(87)   Weigend, F. Accurate Coulomb-Fitting Basis Sets for H to Rn. *Phys. Chem. Chem. Phys.* **2006**, *8* (9), 1057–1065.

(88)   Marenich, A. V.; Cramer, C. J.; Truhlar, D. G. Universal Solvation Model Based on Solute Electron Density and on a Continuum Model of the Solvent Defined by the Bulk Dielectric Constant and Atomic Surface Tensions. *J. Phys. Chem. B* **2009**, *113* (18), 6378–6396.

(89)   Reed, A. E.; Curtiss, L. A.; Weinhold, F. Intermolecular Interactions from a Natural Bond Orbital, Donor—Acceptor Viewpoint. *Chem. Rev.* **1988**, *88* (6), 899–926.

(90)   Janik, M. J.; Taylor, C. D.; Neurock, M. First-Principles Analysis of the Initial Electroreduction Steps of Oxygen over Pt(111). *J. Electrochem. Soc.* **2009**, *156* (1), B126–B135.

(91)   Tripković, V.; Skúlason, E.; Siahrostami, S.; Nørskov, J. K.; Rossmeisl, J. The Oxygen Reduction Reaction Mechanism on Pt(111) from Density Functional Theory Calculations. In *Electrochimica Acta*; 2010; Vol. 55, pp 7975–7981.

(92)   Die, D.; Zheng, B.-X.; Zhao, L.-Q.; Zhu, Q.-W.; Zhao, Z.-Q. Insights into the Structural, Electronic and Magnetic Properties of V-Doped Copper Clusters: Comparison with Pure Copper Clusters. *Sci. Rep.* **2016**, *6* (1), 31978.

(93)   Knight, W. D.; Clemenger, K.; De Heer, W. A.; Saunders, W. A.; Chou, M. Y.; Cohen, M. L. Electronic Shell Structure and Abundances of Sodium Clusters. *Phys. Rev. Lett.* **1984**, *52* (24), 2141–2143.

(94)   Lim, E.; Kim, S. K.; Bowen, K. H. Photoelectron Spectroscopic and Computational Study of (M–CO_2)– Anions, M = Cu, Ag, Au. *J. Chem. Phys.* **2015**, *143* (17), 174305.